Hamiltonian cycles on bicolored random planar maps

Bertrand Duplantier[*] , Olivier Golinelli[†] and Emmanuel Guitter[‡]

Université Paris-Saclay, CEA, CNRS, Institut de Physique Théorique,

91191 Gif-sur-Yvette, France

May 3, 2023

We study the statistics of Hamiltonian cycles on various families of *bicolored* random planar maps (with the spherical topology). These families fall into two groups corresponding to two distinct universality classes with respective central charges $c = -1$ and $c = -2$. The first group includes generic *p-regular* maps with vertices of fixed valency $p \geq 3$, whereas the second group comprises maps with vertices of *mixed* valencies, and the so-called *rigid* case of $2q$-regular maps ($q \geq 2$) for which, at each vertex, the unvisited edges are equally distributed on both sides of the cycle. We predict for each class its universal configuration exponent γ, as well as a new universal critical exponent ν characterizing the number of long-distance contacts along the Hamiltonian cycle. These exponents are theoretically obtained by using the Knizhnik, Polyakov and Zamolodchikov (KPZ) relations, with the appropriate values of the central charge, applied, in the case of ν, to the corresponding critical exponent on regular (hexagonal or square) lattices. These predictions are numerically confirmed by analyzing exact enumeration results for p-regular maps with $p = 3, 4, \ldots, 7$, and for maps with mixed valencies $(2, 3)$, $(2, 4)$ and $(3, 4)$.

1. Introduction

A *planar map* is a connected graph embedded in the two-dimensional sphere without edge crossings, and considered up to homeomorphisms. A map is characterized by its

---

[*]bertrand.duplantier@ipht.fr

[†]olivier.golinelli@ipht.fr

[‡]emmanuel.guitter@ipht.fr

vertices, its edges and its faces which all have the topology of the disk. In this paper, the *size* of a map is defined as its number of vertices. A planar map is *bicolored* if its vertices are colored in black and white so that edges connect only vertices of different colors. A *Hamiltonian cycle* is a closed self-avoiding path drawn along the edges of the map that visits all the vertices of the map. This paper addresses the combinatorial problem of enumerating Hamiltonian cycles on various families of bicolored planar maps. Note that the length of a Hamiltonian cycle on a bicolored map is necessarily an even integer and we shall denote it by $2N$, which is also the size of the underlying map.

For a given family of bicolored planar maps, we will denote by z_N the number of configurations of such maps with size $2N$, equipped with a Hamiltonian cycle and with a *marked visited edge*. The quantity z_N will be referred to as the partition function[1] of the model at hand. At large N, we expect the asymptotic behavior

$$z_N \underset{N \to \infty}{\sim} \varkappa \frac{\mu^{2N}}{N^{2-\gamma}} \ , \tag{1}$$

where $\varkappa$ and μ depend on the precise family of maps we are dealing with, while the *configuration exponent* γ has a more universal nature: as we shall see, only two possible values of γ will be encountered, and it is precisely the aim of this paper to understand when and why one or the other value is observed.

As was done in [1] in the case of *bicubic* maps (i.e., bicolored maps with only 3-valent vertices), we shall argue in the next section that the asymptotic properties of our Hamiltonian cycles on planar bicolored maps may be captured by viewing the problem as the coupling to gravity of a particular critical statistical model described by a conformal field theory (CFT), whose central charge c may itself be deduced from a height reformulation of the problem. More precisely, it is known from the celebrated Knizhnik Polyakov Zamolodchikov (KPZ) formulas [2, 3, 4] that the coupling to gravity of a CFT with central charge $c \leq 1$ corresponds to a fixed size (rooted) partition function z_N with asymptotics (1) where (in the planar case considered in this paper):

$$\gamma = \gamma(c) := \frac{1}{12} \left(c - 1 - \sqrt{(1-c)(25-c)} \right) \ . \tag{2}$$

As it will appear, the various families of bicolored maps that we shall study fall into two categories: when equipped with Hamiltonian cycles, some families will correspond to a CFT with central charge $c = -1$ and therefore exhibit a configuration exponent $\gamma = \gamma(-1) = -(1 + \sqrt{13})/6$, while the other families correspond to a CFT with central charge $c = -2$, leading to a configuration exponent $\gamma = \gamma(-2) = -1$.

In our discussion, it will prove useful to extend our Hamiltonian cycle problem to that, more general, of *fully packed loops* (FPL) on planar bicolored maps. A fully packed loop configuration on a given map is defined as a set of self- and mutually avoiding loops drawn on the edges of the map such that every vertex is visited by a loop. The lengths

---

[1]This should more precisely be called a "rooted partition function" since we decided to mark an edge of the configuration. This marking is convenient as it prevents configurations from having internal symmetries.

of all loops are again even, with total length equal to $2N$, and we finally attach a weight n to each loop: this defines the so-called FPL(n) model on the family of bicolored maps at hand. The case of Hamiltonian cycles may be recovered from the $n \to 0$ limit of the FPL(n) model.

Remark 1. The FPL(n) model itself may be viewed as a particular critical point of the two-dimensional O(n) model. Recall that this latter model describes configurations of self- and mutually avoiding loops with a weight n per loop and a *fugacity x per vertex visited by a loop*. The FPL(n) model is thus recovered within the O(n) model framework by letting $x \to \infty$ so that all vertices be visited by a loop. As we shall recall later, the FPL(n) model is intimately linked to the *dense critical phase* of the O(n) model.

Remark 2. Let us insist on the fact that *all the maps that we consider in this paper are bicolored*. As explained in [5, 1], this coloring constraint is crucial when it comes to identifying the central charge of the associated CFT. We will comment on this in Remark 10 below.

We also address the question of long-distance contacts within Hamiltonian cycles on random planar maps. Marking two points at distance N along a cycle splits the latter into two equal parts, and defines a set of *contact links*, i.e., edges that are incident to *both* parts of the cycle; these contact links can be seen as connected by a *dual contact cycle* on the dual map. Their average number scales as N^ν, with a new exponent ν depending on the underlying map family. The values of ν are predicted theoretically by using, for the proper value of the central charge c, the KPZ formula applied to a similar exponent on regular (hexagonal or square) lattices, which is (half) the Hausdorff dimension of contacts within a loop of the regular FPL($n \to 0$) model. As we shall see, in the scaling limit, a bicolored random planar map equipped with a Hamiltonian cycle is expected to converge to a *Liouville quantum gravity (LQG) sphere* [6], decorated by an *independent (space-filling) whole-plane Schramm-Loewner evolution* SLE$_8$ [7], the dual contact cycle itself converging to a dual *whole-plane* SLE$_2$. The LQG parameter is $\gamma_{\mathrm{L}} = 2/\sqrt{1 - \gamma}$, with either $\gamma = \gamma(c = -1)$ or $\gamma = \gamma(c = -2)$, depending on the chosen map's family. These predictions are in the same spirit as those made in Refs. [1, 8, 9].

The paper is organized as follows: Section 2 discusses Hamiltonian cycles on bicolored planar maps whose *all vertices have the same valency* and gives our prediction for the configuration exponent γ in this case. Section 3 deals on the contrary with the case of maps having several allowed vertex valencies, leading to another value of γ. The predictions of these two sections are verified numerically in Section 4 by analyzing exact enumeration results for maps of finite sizes. Section 5 introduces the notion of *rigid* Hamiltonian cycles and predicts a configuration exponent different from that of the non-rigid case. This result is confirmed by the derivation of exact expressions for z_N for arbitrary N. Section 6 addresses the question of long-distance contacts within Hamiltonian cycles, whose average number scales as N^ν with the exponent ν depending on the underlying map family. Two possible values of ν are predicted theoretically and then checked numerically in Section 7. We conclude with a few remarks in Section 8.
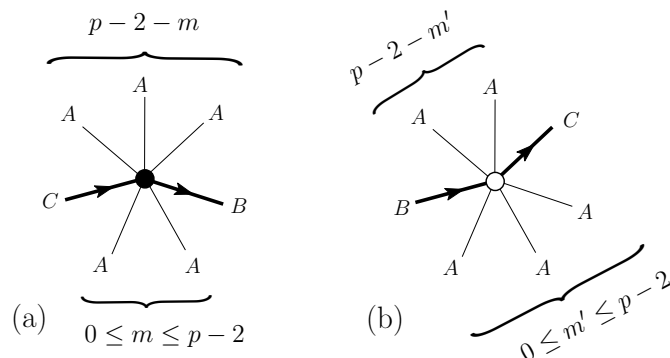
3

Figure 1: Example of the edge environment of (a) a black vertex and (b) a white vertex. Each vertex is surrounded by a B-edge, a C-edge and a total of $(p-2)$ A-edges (here $p = 7$, $m = 2$ and $m' = 3$).

2. The case of p-regular bicolored maps

Recall that a *p-regular map* is a map whose all vertices have valency p. This section is devoted to the enumeration of Hamiltonian cycles on p-regular bicolored planar maps for a fixed integer $p \geq 3$. It includes in particular the case of bicubic maps ($p = 3$) studied in [1, 5].

From now on, we therefore assume that p takes a fixed value and we start by considering the FPL(2) model on p-regular bicolored planar maps. Assigning the weight $n = 2$ per loop amounts equivalently to having unweighted *oriented* loops (the weight 2 arising then from the 2 possible orientations for each loop). This allows us to define three types of edges (see Figure 1): the unvisited edges, called A-edges, the edges visited by a loop whose orientation points toward their white incident vertex, which we call B-edges, and finally the edges visited by a loop whose orientation points toward their black incident vertex, which we call C-edges. The configuration of edges around a black vertex is then that of Figure 1-(a) with an ingoing C-edge, an outgoing B-edge and a total of $p - 2$ unvisited A-edges which are distributed in all possible ways on both sides of the loop. Similarly, the configuration of edges around a white vertex is that of Figure 1-(b) with now an ingoing B-edge, an outgoing C-edge and $p - 2$ unvisited A-edges.

We may now transform the FPL(2) model into a *d-component height model* by assigning a height $\boldsymbol{X} \in \mathbb{R}^d$ to each face of the map, whose variation $\Delta \boldsymbol{X}$ between adjacent faces depends on the nature of the edge between them according to the rules of Figure 2: we demand that $\Delta \boldsymbol{X} = \boldsymbol{A}$ (resp. $\boldsymbol{B}$, $\boldsymbol{C}$) if the crossed edge is of type A (resp. B, C) and traversed with its incident white vertex on the right. To guarantee that the height is well defined across the whole map, we have to ensure that we recover the same value of $\boldsymbol{X}$ after making a complete turn around any vertex of the map. This requires (see Figure 2) the necessary and sufficient condition:

$$(p - 2)\boldsymbol{A} + \boldsymbol{B} + \boldsymbol{C} = \boldsymbol{0} \tag{3}$$

which, de facto, implies that $\boldsymbol{X}$ lives in the $(\boldsymbol{B}, \boldsymbol{C})$ *two-dimensional* plane. For definite-
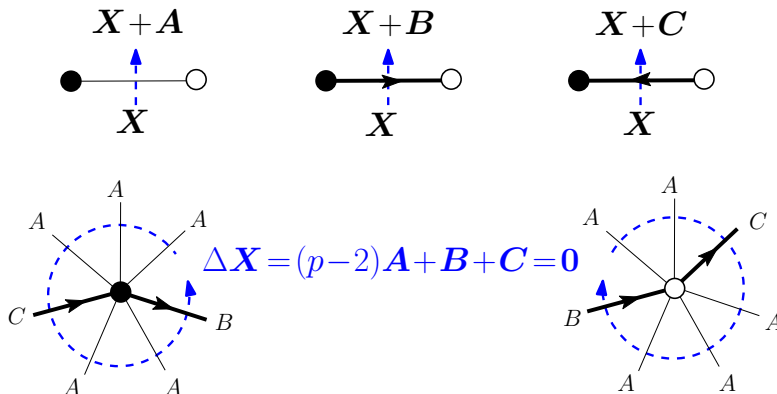
Figure 2: Top: rules for the variation in the height variable $\boldsymbol{X}$ when crossing an edge of the map. Bottom: making a complete turn counterclockwise (resp. clockwise) around a black (resp. white) vertex results in a height variation $\Delta\boldsymbol{X} = (p-2)\boldsymbol{A} + \boldsymbol{B} + \boldsymbol{C}$ which for consistency must be taken equal to $\boldsymbol{0}$.

ness, we choose $d = 2$ with $\boldsymbol{B}$ and $\boldsymbol{C}$ two unit vectors of $\mathbb{R}^2$ satisfying, say $\boldsymbol{B}\cdot\boldsymbol{C} = -1/2$. In particular, the property $|\boldsymbol{B}| = |\boldsymbol{C}|$ implies that $(\boldsymbol{B}-\boldsymbol{C})\cdot(\boldsymbol{B}+\boldsymbol{C}) = 0$ hence, if we define

$$\boldsymbol{b_2} := \boldsymbol{B} - \boldsymbol{C} \ , \tag{4}$$

we deduce from (3) that $\boldsymbol{A}\cdot\boldsymbol{b_2} = 0$ and a natural convention consists in expressing our two-component height variable $\boldsymbol{X}$ in the *orthogonal* basis $(\boldsymbol{A}, \boldsymbol{b_2})$. In the continuous limit, we expect that the FPL(2) model is therefore described by the coupling to gravity of a two-dimensional CFT involving a *two-component vector field* $\boldsymbol{\Psi} = \psi_1\boldsymbol{A} + \psi_2\boldsymbol{b_2}$ (i.e., with components both along $\boldsymbol{A}$ and along $\boldsymbol{b_2}$) measuring locally the "coarse grained" averaged value $\boldsymbol{\Psi} = \langle\boldsymbol{X}\rangle$ and governed by a free field action for both ψ_1 and ψ_2, see [1]. We deduce the following:

Claim 3. *The FPL(2) model on p-regular bicolored planar maps is described by the coupling to gravity of a CFT with central charge*

$$c = 2 \ . \tag{5}$$

We now wish to understand how this result is modified if we give an arbitrary weight n to each loop, hence consider the FPL(n) model on p-regular bicolored planar maps. The case $p = 3$ of bicubic maps was discussed in details in [1]. There, the underlying CFT is identified as that describing the FPL(n) model on the *honeycomb, i.e., hexagonal lattice* (which is 3-regular and can be bicolored canonically), a model well studied in [10, 11, 12, 13] by Bethe Ansatz or Coulomb gas techniques. For this lattice model, the passage from $n = 2$ to an arbitrary $n \in [-2, 2]$ modifies in the continuous limit the Gaussian free field action by adding a term which couples the component ψ_2 of the two-component field $\boldsymbol{\Psi}$ to the local intrinsic curvature of the underlying surface, while the action for the component ψ_1 remains that of a free field. For $n \in [-2, 2]$, the net
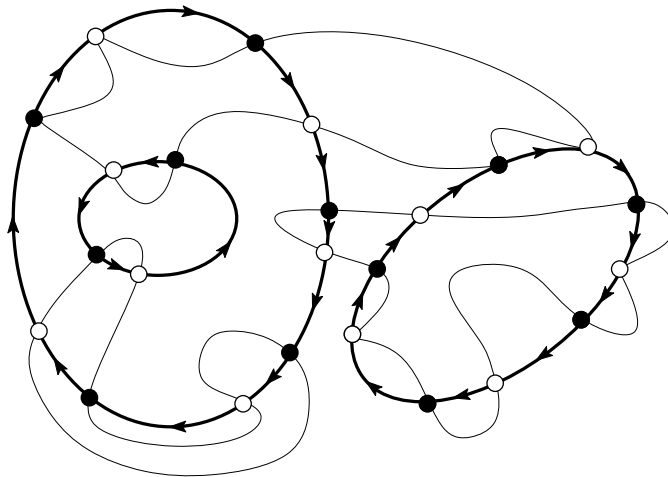
Figure 3: An example of a 4-regular bicolored planar map equipped with a set of fully packed oriented loops (thick lines). The unvisited edges (thin lines) automatically form a complementary set of fully packed unoriented loops on the map.

result is a shift of the central charge from $c = c_{\mathrm{fpl}}(2) = 2$ to a lower value $c = c_{\mathrm{fpl}}(n)$ [11] whose expression is recalled just below.

Since the FPL(2) model on p-regular bicolored planar maps has the same two-component field description for any arbitrary integer $p \geq 3$, we expect that the passage from $n = 2$ to an arbitrary $n \in [-2, 2]$ induces the very same lowering of the central charge. This leads us to express the following statement:

Claim 4. *For $-2 \leq n \leq 2$, the FPL(n) model on p-regular bicolored planar maps is, for arbitrary $p \geq 3$, described by the coupling to gravity of a CFT with central charge*

$$c = c_{\mathrm{fpl}}(n) := 2 - 6\frac{(1-g)^2}{g} \quad \text{where } n = -2\cos(\pi\, g) \text{ with } 0 \leq g \leq 1 \ . \tag{6}$$

In the $n \to 0$ limit, we deduce in particular:

Corollary 5. *The model of Hamiltonian cycles on p-regular bicolored planar maps is described by the coupling to gravity of a CFT with central charge*

$$c = c_{\mathrm{fpl}}(0) = -1 \ . \tag{7}$$

In particular, using KPZ (2), the partition function z_N of Hamiltonian cycles on p-regular bicolored planar maps of size $2N$ has the asymptotic behavior (1) with

$$\gamma = \gamma(-1) = -\frac{1 + \sqrt{13}}{6} \ . \tag{8}$$

This extends the conjecture of [5] (see also [14, 1]) for $p = 3$ to an arbitrary value of the integer $p \geq 3$.

It is interesting to remark that for $p = 4$ we may arrive at the statements of Claim 4 and Corollary 5 by a different route as follows. For $p = 4$, each vertex is incident to exactly 2 unvisited edges: the unvisited edges thus naturally form loops visiting all the vertices of the bicolored map, see Figure 3. We therefore have by construction two complementary systems of fully packed loops: the original fully packed loops which receive a weight $n_1 = n$ and the loops formed by the unvisited edges which receive the neutral weight $n_2 = 1$. The FPL(n) model on 4-regular bicolored planar maps may therefore be viewed as a particular instance of the coupling to gravity of the so-called FPL$^2(n_1, n_2)$ model, which involves two complementary fully packed loop systems with respective weights n_1 and n_2 on the square lattice (which is 4-regular and can be bicolored canonically). The FPL$^2(n_1, n_2)$ model on this lattice was studied in details in [15, 16, 17, 18] by Coulomb gas and Bethe Ansatz techniques. Its central charge was found to equal $c_{\mathrm{fpl}^2}(n_1, n_2) = 3 - 6(1 - g_1)^2/g_1 - 6(1 - g_2)^2/g_2$ where, for $i = 1, 2$, $n_i = -2\cos(\pi g_i)$ with $0 \leq g_i \leq 1$. Taking $g_1 = g$ as in (6) and $g_2 = 2/3$ so that $(n_1, n_2) = (n, 1)$, we recover the value $c_{\mathrm{fpl}^2}(n, 1) = 2 - 6(1 - g)^2/g = c_{\mathrm{fpl}}(n)$ as in Claim 4 and Corollary 5 .

Note that, for $p \geq 5$, we can no longer rely on hypothetical results for a fully packed loop model on some regular lattice, since there exists no such bicolored regular lattice with p-valent vertices only[2]. Moreover, for $p \geq 5$, there is no canonical way to arrange the unvisited edges into loops, would it be only for a subset of these unvisited edges.

3. The case of bicolored maps with mixed valencies

In this section, we deal with planar maps whose vertices have valencies within the fixed set $\mathcal{S} = \{p_1, p_2, \ldots, p_k\}$ where $k \geq 2$ and where the integers p_i satisfy $2 \leq p_1 < p_2 < \cdots < p_k$. Such maps will be generically referred to as *maps with mixed valencies*. Again we are interested in evaluating the number of such bicolored maps equipped with a Hamiltonian cycle, or more generally a set of fully packed loops with a weight n per loop. Since the (self- and mutually-avoiding) loops visit all the vertices, the underlying maps have by construction an even size $2N$, with exactly N black and N white vertices. The statistical ensemble that we consider is that *with fixed* N and with a weight $w_i \in \mathbb{R}^+$ attached to each vertex with valency p_i. We insist here on the fact that the numbers m_i of vertices of valency p_i are not fixed individually but that their sum $m_1 + m_2 + \cdots + m_k = 2N$ is fixed. We call z_N the associated partition function with, as before, a marked visited edge. The partition function z_N depends implicitly on the set $\mathcal{S}$ and on the weights w_i. Note that, since $w_i > 0$ for all $i \in \{1, \ldots, k\}$, we expect the average number of vertices $\langle m_i \rangle = w_i \frac{\partial}{\partial w_i} \mathrm{Log} z_N$ to be of order N for all i's, i.e., extensive for each valency p_i.

As in the previous section, we start by studying the FPL(2) model on our bicolored maps with mixed valencies and fixed size $2N$. As before, the weight 2 per loop can be realized by orienting the loops, and we may again describe alternatively the configurations by a d-component height variable $\boldsymbol{X} \in \mathbb{R}^d$ defined from the loop content according to

---

[2]For $p = 6$, a natural candidate with only 6-regular vertices is the triangular lattice but this lattice is not bicolorable.

the rules of Figure 2-top. Note that configurations where valencies belong only to a proper subset of $\mathcal{S}$ may appear. However, since all weights w_i, $i \in \{1, 2, \ldots, k\}$ have been chosen to be strictly positive, the asymptotic behavior of the partition function z_N is exponentially dominated by configurations where all valencies are *macroscopically* present. Considering two different valencies, say p_{i_1} and p_{i_2}, we must, in order to have a well defined uni-valued height, impose simultaneously the two conditions $(p_{i_1}-2)\boldsymbol{A}+\boldsymbol{B}+\boldsymbol{C}=\boldsymbol{0}$ (necessary around a vertex of valency p_{i_1}) and $(p_{i_2}-2)\boldsymbol{A}+\boldsymbol{B}+\boldsymbol{C}=\boldsymbol{0}$ (necessary around a vertex of valency p_{i_2}). Since we assumed $p_{i_1} \neq p_{i_2}$, these two conditions imply

$$\boldsymbol{A}=\boldsymbol{0} \quad \text{and} \quad \boldsymbol{B}+\boldsymbol{C}=\boldsymbol{0} \ . \tag{9}$$

This now implies that $\boldsymbol{X}$ stays colinear to $\boldsymbol{B}$, or equivalently to $\boldsymbol{b_2} := \boldsymbol{B}-\boldsymbol{C}=2\boldsymbol{B}$. In the continuous limit, we expect that the FPL(2) model is now described by the coupling to gravity of a two-dimensional CFT involving a *one-component field* $\boldsymbol{\Psi} = \psi_2 \boldsymbol{b_2}$ (i.e., with a components along $\boldsymbol{b_2}$ only, so that we may in practice fix $d = 1$) measuring as before the "coarse grained" averaged value $\boldsymbol{\Psi} = \langle \boldsymbol{X} \rangle$ and governed by a Gaussian free field action. This leads us to the following:

Claim 6. *The FPL(2) model on bicolored planar maps with mixed valencies is described by the coupling to gravity of a CFT with central charge*

$$c = 1 \ . \tag{10}$$

As for the case of arbitrary $n \in [-2, 2]$, the action of the associated continuous CFT is again obtained by adding to the free field action for ψ_2 a term which couples it to the local intrinsic curvature of the underlying surface. Since there is no component ψ_1 anymore, the obtained central charge becomes equal to $c = c_{\text{dense}}(n) := c_{\text{fpl}}(n) - 1$. We arrive at:

Claim 7. *For $-2 \leq n \leq 2$, the FPL(n) model on bicolored planar maps with mixed valencies is described by the coupling to gravity of a CFT with central charge*

$$c = c_{\text{dense}}(n) := 1 - 6\frac{(1-g)^2}{g} \quad \text{where } n = -2\cos(\pi\, g) \text{ with } 0 \leq g \leq 1 \ . \tag{11}$$

In the $n \to 0$ limit, we deduce in particular:

Corollary 8. *The model of Hamiltonian cycles on bicolored planar maps with mixed valencies is described by the coupling to gravity of a CFT with central charge*

$$c = c_{\text{dense}}(0) = -2 \ . \tag{12}$$

In particular, using KPZ, the associated partition function z_N has the asymptotic behavior (1) with
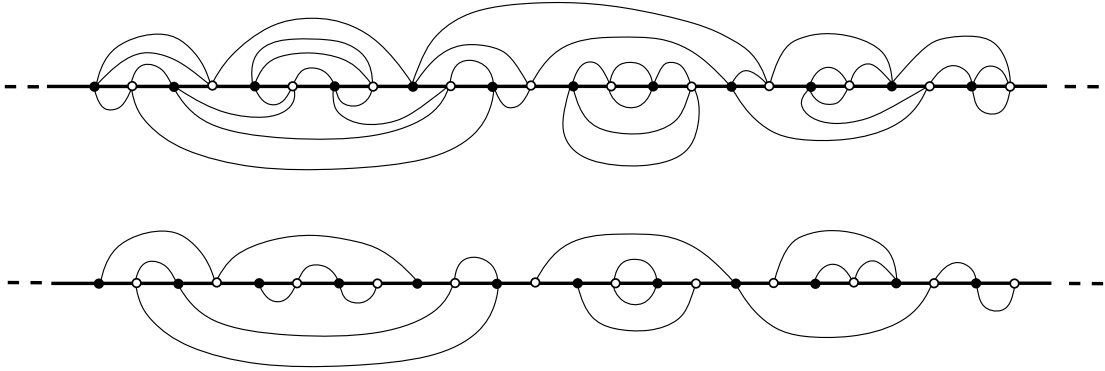
$$\gamma = \gamma(-2) = -1 \ . \tag{13}$$

Figure 4: Representation of a Hamiltonian cycle (after opening its marked visited edge) as an infinite straight line with alternating black and white vertices, connected by non-crossing bicolored arches on both sides of the infinite line. Top: example in the p-regular case with $p = 5$. Bottom: example in the case of mixed valencies 3 and 4, i.e., $k = 2$ and $\mathcal{S} = \{3, 4\}$.

Remark 9. The denomination "dense" refers to the fact that the value $c_{\mathrm{dense}}(n)$ of the central charge is precisely that associated with the two-dimensional $\mathrm{O}(n)$ model in its dense critical phase, where the number of occupied vertices is macroscopic, with loops being no longer required to visit all the vertices (see Section 6.1 for a detailed discussion). Here we recover this value even though, in our problem, loops by definition visit all vertices. The randomness due to the multiple choice of valencies somehow erases the full-packing constraint, which corresponds to an unstable manifold in the parameter space of the $\mathrm{O}(n)$ model [11].

Remark 10. Note that a similar reduction in the central charge from $c_{\mathrm{fpl}}(n)$ to $c_{\mathrm{dense}}(n) = c_{\mathrm{fpl}}(n) - 1$ would be observed for p-regular maps in the absence of the bicoloring constraint. Indeed, in that case, it is no longer possible to distinguish the two sides of an A-edge (see Figure 2-top), which forces one to set $\boldsymbol{A} = \boldsymbol{0}$ and thus $\boldsymbol{B} + \boldsymbol{C} = \boldsymbol{0}$ as in (9); see [1] for a detailed discussion in the 3-regular map case.

4. Numerical verification

In order to verify the claims of Corollaries 5 and 8, we performed a direct numerical enumeration of Hamiltonian cycles on various p-regular map families as well as on various families of maps with mixed valencies. In all cases, by cutting the Hamiltonian cycle at the level of its marked visited edge and opening it into a straight line, we obtain a configuration of the form of that in Figure 4, with an infinite line carrying $2N$ alternating black and white vertices. A vertex of valency p_i leads to a total number $(p_i - 2)$ of incident unvisited half-edges distributed in all possible ways on both sides of the infinite line. Finally, these half-edges are connected in pairs so as to form a set of *bicolored non-crossing arches*. To obtain the value of the number of possible configurations z_N for a given map family, we use a transfer matrix approach, generalizing that of [1], in which
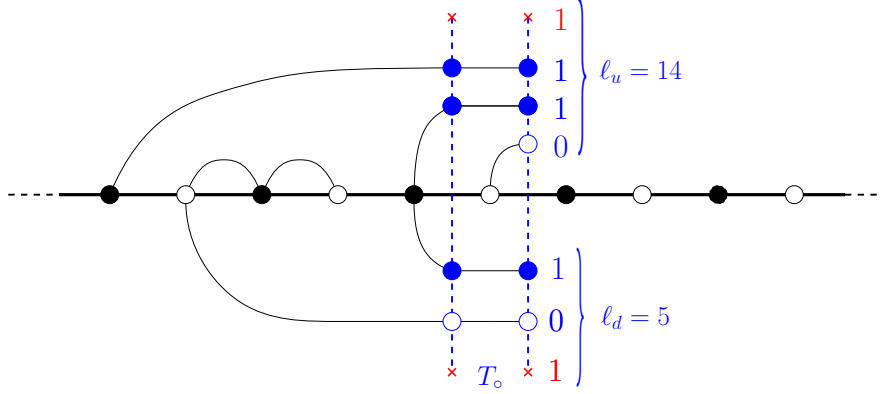
Figure 5: Illustration of the transfer matrix method in the case of mixed valencies with $\mathcal{S} = \{3, 4\}$. Here we display one of the possible outcomes for the action of the elementary transfer matrix $T_\circ$ at the crossing of a white vertex.

the arch configurations are built from left to right along the straight line of alternating black and white vertices. A transfer matrix state is described by the color sequence of those arches which have been opened but not yet closed, each arch inheriting the color of the vertex it originates from (see Figure 5). The upper arch color sequence is read from bottom to top and the lower one from top to bottom. A sequence of s arches with colors $a_1, \ldots, a_s$ (where we choose $a_j = 1$ for black and 0 for white) is encoded by the integer $\ell = 2^s + \sum_{j=1}^{s} a_j 2^{(j-1)}$ so that a transfer matrix intermediate state is coded by two positive integers ℓ_u (upper sequence) and ℓ_d (lower sequence) and denoted as $|\ell_u, \ell_d\rangle$. With these notations, the partition function z_N may be written as

$$z_N = \langle 1, 1| (T_\circ T_\bullet)^N |1, 1\rangle \tag{14}$$

where $|1, 1\rangle$ correspond to the empty configuration (the vacuum state) while $T_\bullet$ and $T_\circ$ are two elementary transfer matrices transferring the state respectively across a black and a white vertex. Note that, for N even, we may write

$$\begin{aligned} z_N &= \sum_{\ell_u, \ell_d} \langle 1, 1| (T_\circ T_\bullet)^{N/2} |\ell_u, \ell_d\rangle \langle \ell_u, \ell_d| (T_\circ T_\bullet)^{N/2} |1, 1\rangle \\ &= \sum_{\ell_u, \ell_d} \left(\langle \ell_u, \ell_d| (T_\circ T_\bullet)^{N/2} |1, 1\rangle \right)^2 , \end{aligned} \tag{15}$$

where the sum is over the *finite* number of reachable states after N steps ($N/2$ of each color). Here we used the symmetry of the problem under combined left-right reversal and black-white inversion of vertex colors. Similarly, for N odd, we have

$$\begin{aligned} z_N &= \sum_{\ell_u, \ell_d} \langle 1, 1| (T_\circ T_\bullet)^{(N-1)/2} T_\circ |\ell_u, \ell_d\rangle \langle \ell_u, \ell_d| T_\bullet (T_\circ T_\bullet)^{(N-1)/2} |1, 1\rangle \\ &= \sum_{\ell_u, \ell_d} \left(\langle \ell_u, \ell_d| T_\bullet (T_\circ T_\bullet)^{(N-1)/2} |1, 1\rangle \right)^2 . \end{aligned} \tag{16}$$
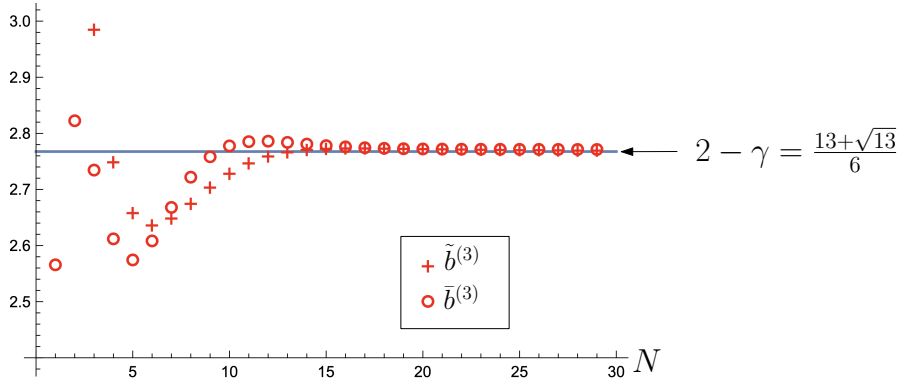
10

Figure 6: Estimates of $2 - \gamma$ for Hamiltonian cycles on 3-regular bicolored planar maps, as obtained from the associated accelerated series $\tilde{b}_N^{(3)}$ and $\bar{b}_N^{(3)}$ defined in (17) and (18). These estimates confirm and extend the results of [5] and [1].

We therefore see that, for both parities and for a total size $2N$ of the map configuration, we only have to perform the action of N elementary transfer matrices.

From z_N, we may obtain μ and γ in (1) as the limits of appropriate sequences: for instance the sequence

$$b_N := N^2 \, \mathrm{Log} \frac{z_{N+2} z_N}{(z_{N+1})^2} \tag{17}$$

tends to $2 - \gamma$ for $N \to \infty$. We may therefore get an estimate for γ from the value of b_N for some finite, large enough, N. To get a better estimate, we also have recourse to *series acceleration methods*, involving sequences constructed from b_N by recursive use of the finite difference operator Δ (defined by $(\Delta f)_N := f_{N+1} - f_N$) and which converge faster to the same limit $2 - \gamma$ as $N \to \infty$. In practice, we use the two "accelerated" series $\tilde{b}_N$ and $\bar{b}_N$ defined as[3]

$$\begin{aligned} \tilde{b}_N &:= \frac{1}{3!} (\Delta^3 \hat{b})_N \quad \text{with} \quad \hat{b}_N := N^3 b_N \;, \\ \bar{b}_N &:= b_{N+2} - 2 \frac{(\Delta b)_{N+2} (\Delta b)_{N+1}}{(\Delta^2 b)_{N+1}} \;. \end{aligned} \tag{18}$$

Appendix B presents our numerical results for the enumeration of z_N. More precisely, we deal with the following map families:

- p-regular bicolored planar maps for $p = 3, 4, \ldots, 7$;

- bicolored planar maps with mixed valencies for $\mathcal{S} = \{2, 3\}, \{2, 4\}$ with weights $w_2 = w_3 = w_4 = 1$ and for $\mathcal{S} = \{3, 4\}$ with $(w_3, w_4) = (1, 1), (1, 2)$ and $(2, 1)$.

From these values, we extract the estimates of μ^2 listed in Table 1.

Figures 6 and 7 present our estimates of $2 - \gamma$ for the p-regular bicolored planar maps with $p = 3$ and $p = 4$ to 7 respectively (for each p, we denote by $b_N^{(p)}$ the associated series

---

[3]The two series are defined so that their N'th element involves values of z_M for M up to $N + 5$.
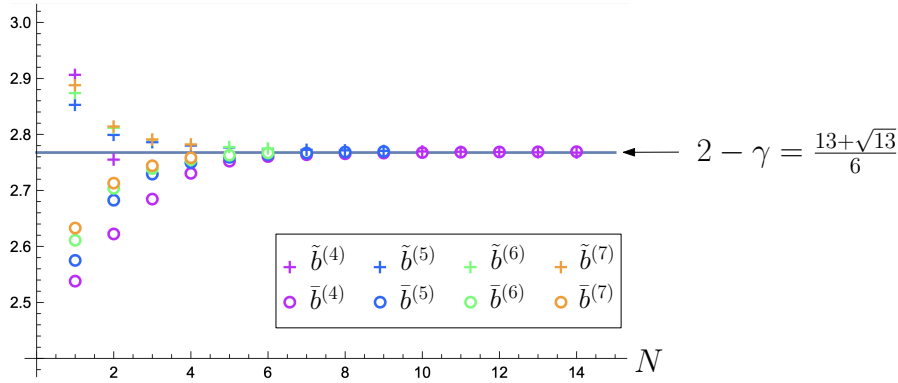
Figure 7: Estimates of $2 - \gamma$ for Hamiltonian cycles on p-regular bicolored planar maps, as obtained from the associated accelerated series $\tilde{b}_N^{(p)}$ and $\bar{b}_N^{(p)}$ for $p = 4, 5, 6,$ and 7.

p-regular maps	μ^2	maps with mixed valencies		μ^2
3-regular	10.113 ± 0.001	$\{2,3\}$	$(w_2 = w_3 = 1)$	16.204 ± 0.001
4-regular	41.60 ± 0.02	$\{2,4\}$	$(w_2 = w_4 = 1)$	49.9 ± 0.1
5-regular	117.0 ± 0.2	$\{3,4\}$	$(w_3 = w_4 = 1)$	86.02 ± 0.05
6-regular	$265.5 \pm 1.$	$\{3,4\}$	$(w_3 = 1 , w_4 = 2)$	244.0 ± 0.2
7-regular	$522.8 \pm 2.$	$\{3,4\}$	$(w_3 = 2 , w_4 = 1)$	151.0 ± 0.2

Table 1: Estimated values of the exponential growth factor μ^2.

(17)). These estimates are in perfect agreement with the expected value $\gamma = -(1+\sqrt{13})/6$ of Corollary 5.

Figure 8 presents our estimates of $2 - \gamma$ for bicolored planar maps with mixed valencies for $\mathcal{S} = \{2,3\}$ and $\{2,4\}$ (with all weights $w_i = 1$) while Figure 9 presents our estimates for bicolored planar maps with mixed valencies in $\mathcal{S} = \{3,4\}$ with $(w_3, w_4) = (1,1), (1,2)$ and $(2,1)$ respectively. The estimates now agree with the expected value $\gamma = -1$ of Corollary 8.

5. Rigid Hamiltonian cycles on $2q$-regular bicolored planar maps

5.1. Definition and properties

Let us now discuss a restricted class of Hamiltonian cycles, or more generally of fully packed loops, which, as in [19], we call *rigid*. Those are defined as follows: a rigid fully packed loop (RFPL) configuration is a set of fully packed loops on a $2q$-regular bicolored planar map, with $q \geq 2$ a fixed integer, such that, at each vertex, the unvisited edges are equally distributed on both sides of the loop, i.e., with exactly $(q - 1)$ of them on each side, see Figure 10. As before, each loop receives a weight n: this defines the RFPL(n) model on $2q$-regular bicolored planar maps. Again the $n \to 0$ limit selects configurations
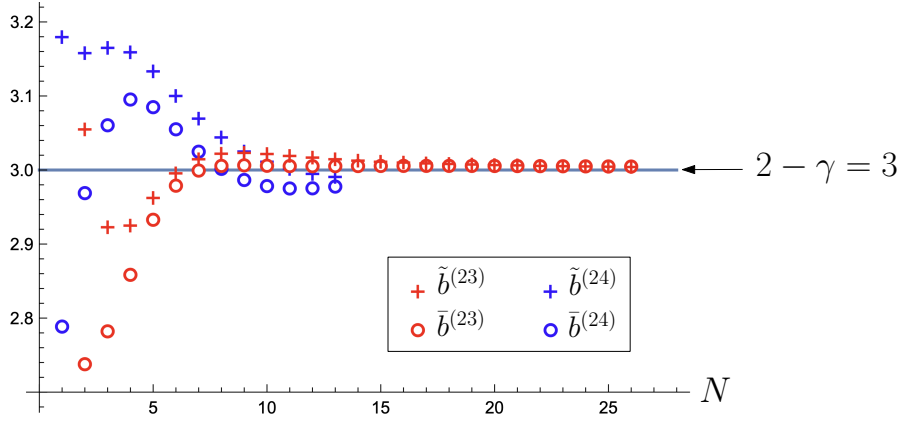
Figure 8: Estimates of $2 - \gamma$ for Hamiltonian cycles on bicolored planar maps with mixed valencies in $\mathcal{S} = \{2,3\}$ (accelerated series $\tilde{b}_N^{(23)}$ and $\bar{b}_N^{(23)}$ with $w_2 = w_3 = 1$) and in $\mathcal{S} = \{2,4\}$ (accelerated series $\tilde{b}_N^{(24)}$ and $\bar{b}_N^{(24)}$ with $w_2 = w_4 = 1$).
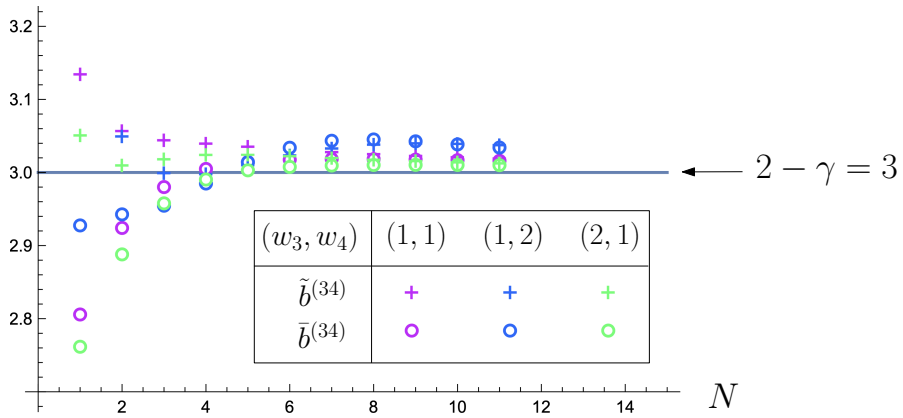

Figure 9: Estimates of $2 - \gamma$ for Hamiltonian cycles on bicolored planar maps with mixed valencies in $\mathcal{S} = \{3,4\}$ with $(w_3, w_4) = (1,1), (1,2)$ and $(2,1)$ respectively.
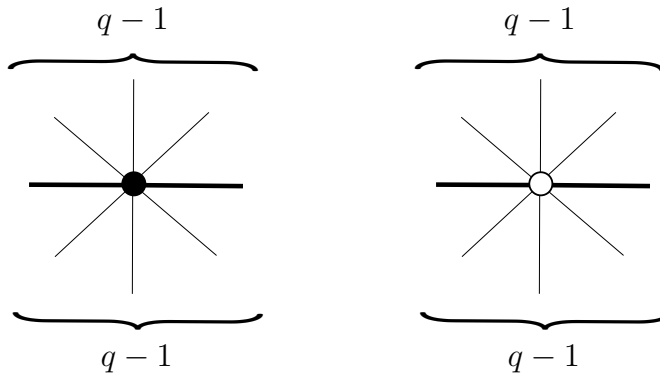
13

Figure 10: Example of the edge environment of a black and of a white vertex in the RFPL model. Each vertex is traversed by a loop (thick edges) in such a way that there are exactly $q-1$ unvisited edges (thin edges) on each side of the loop (here $q = 4$).

of *rigid Hamiltonian cycles*, i.e., configurations with a single self-avoiding loop visiting all the vertices of the map.

For $2q = 4$, a rigid Hamiltonian cycle configuration is what was called a *meandric system* in [20, 9]. Note that a 4-regular planar map equipped with a rigid Hamiltonian cycle is automatically bicolorable.

Let us again start with the RFPL(2) model, corresponding to (unweighted) oriented loops. As we did in Section 2, we may distinguish A- (unvisited), B- (visited oriented towards a black vertex) and C- (visited oriented towards a black vertex) edges, which allows us to assign a d-component height $\boldsymbol{X} \in \mathbb{R}^d$ to each face of the map, whose variation $\Delta \boldsymbol{X}$ between adjacent faces depends on the nature of the edge between them according to the rules of Figure 2. As before, this height is well-defined by requiring the necessary and sufficient condition (corresponding to (3) for $p = 2q$):

$$2(q-1)\boldsymbol{A} + \boldsymbol{B} + \boldsymbol{C} = \boldsymbol{0} \tag{19}$$

which, de facto, fixes $d = 2$, with $\boldsymbol{X}$ living in the $(\boldsymbol{B}, \boldsymbol{C})$-plane with $\boldsymbol{B}$ and $\boldsymbol{C}$ two unit vectors with, say $\boldsymbol{B} \cdot \boldsymbol{C} = -1/2$. As before, it is convenient to express $\boldsymbol{X}$ in the orthogonal basis $(\boldsymbol{A}, \boldsymbol{b_2})$, with $\boldsymbol{b_2} := \boldsymbol{B} - \boldsymbol{C}$ and, as in Section 2, write the associated coarse grained average value $\boldsymbol{\Psi} = \langle \boldsymbol{X} \rangle$ as a two-component vector field $\boldsymbol{\Psi} = \psi_1 \boldsymbol{A} + \psi_2 \boldsymbol{b_2}$ with components both along $\boldsymbol{A}$ and along $\boldsymbol{b_2}$. Reproducing the arguments of Section 2, it would be tempting to infer that the results of Claims 3 and 4 hold, i.e., that the RFPL(n) model is the coupling to gravity of a CFT of central charge $c_{\text{fpl}}(n)$. We will now argue that this conclusion is actually incorrect and that the RFPL(n) model is the coupling to gravity of a CFT of central charge $c_{\text{dense}}(n) = c_{\text{fpl}}(n) - 1$. Indeed, even though we may define the coordinate ψ_1 in the $\boldsymbol{A}$ direction, the value of this coordinate is in practice *frozen*, equal to a fixed value (which we may take equal to 0) on the entire map. We thus state:

Proposition 11. *The two-component vector field $\boldsymbol{\Psi}$ varies only via its coordinate ψ_2 along the $\boldsymbol{b_2}$ direction, which makes it in practice a one-component vector field.*

This de facto reduces the central charge by 1, hence we arrive at:

Claim 12. *For $-2 \leq n \leq 2$, the RFPL(n) model on $2q$-regular bicolored planar maps is described by the coupling to gravity of a CFT with central charge*

$$c = c_{\text{dense}}(n) = 1 - 6\frac{(1-g)^2}{g} \quad \text{where } n = -2\cos(\pi g) \text{ with } 0 \leq g \leq 1 . \quad (20)$$

In the $n \to 0$ limit, we deduce in particular:

Corollary 13. *The model of rigid Hamiltonian cycles on $2q$-regular bicolored planar maps is described by the coupling to gravity of a CFT with central charge*

$$c = c_{\text{dense}}(0) = -2 . \quad (21)$$

In particular, using KPZ (2)*, the associated partition function z_N has the asymptotic behavior* (1) *with*

$$\gamma = \gamma(-2) = -1. \quad (22)$$

5.2. Proof of Proposition 11

Proof. The following argument is a generalization to arbitrary q of that given in [14, Sect. 11.3] for the case $q = 2$. The first remark is that the set of faces of a bicolored p-regular planar map is naturally split into p subsets as follows[4]: pick a reference face f_0 and label each face f of the map by $\ell(f) = (L(f) \mod p) + 1$ where $L(f)$ is the number of crossed edges of any path connecting f_0 to f and *traversing only edges with their white vertex on the right* (or equivalently turning clockwise around white vertices and counterclockwise around black ones). It is easily seen that $L(f)$ is indeed independent on the chosen path. This splits the set of faces into p-subsets which we denote by $\mathcal{F}_1, \mathcal{F}_2, \ldots, \mathcal{F}_p$ where $\mathcal{F}_j$ is the set of faces labelled j. Moreover, it is easily seen that, by construction, the cyclic order of the labels is $(1, 2, \ldots, p)$ both clockwise around white vertices and counterclockwise around black ones. For $p = 2q$, we may instead use labels $\ell \in \{1, 2, \ldots, q, \hat{1}, \hat{2}, \ldots, \hat{q}\}$ so that the subsets are now denoted by $\mathcal{F}_1, \mathcal{F}_2, \ldots, \mathcal{F}_q, \mathcal{F}_{\hat{1}}, \mathcal{F}_{\hat{2}}, \ldots, \mathcal{F}_{\hat{q}}$ and the cyclic order of the labels is $(1, 2, \ldots, p, \hat{1}, \hat{2}, \ldots, \hat{q})$. In the presence of rigid fully packed oriented loops, we may finally choose the face f_0 so that the loops always separate faces in $\mathcal{F}_1$ from faces in $\mathcal{F}_{\hat{q}}$ and faces in $\mathcal{F}_{\hat{1}}$ from faces in $\mathcal{F}_q$ (it is enough to impose this property at one vertex and, since the loops are rigid, it automatically propagates[5] to all the vertices), see Figure 11 for an example in the case $q = 3$.

---

[4]The reader might be more familiar with the dual picture: bicolored p-regular planar maps are dual to planar Eulerian p-angulations (with bicolored black and white faces all of valency p), a particular instance of p-constellations [21].

[5]Note that the set $\mathcal{F}_1 \cup \mathcal{F}_{\hat{1}}$ needs not be connected. Still, one can check that the property propagates from one connected component to the other. This is because the edges separating $\mathcal{F}_j$ from $\mathcal{F}_{j-1}$ and $\mathcal{F}_{\hat{j}}$ from $\mathcal{F}_{\widehat{j-1}}$ for any given $j \in \{2, \ldots q\}$ also form a set of rigid fully packed loops.
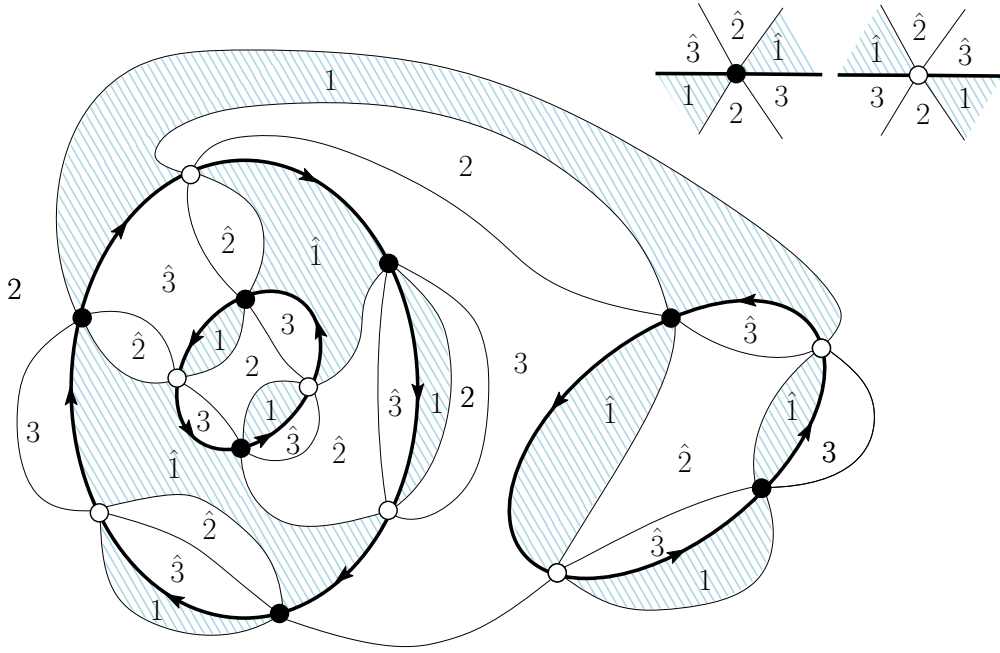
Figure 11: The splitting of the face set into subsets $\mathcal{F}_1, \mathcal{F}_2, \mathcal{F}_3, \mathcal{F}_{\hat{1}}, \mathcal{F}_{\hat{2}}, \mathcal{F}_{\hat{3}}$ for a 6-regular bicolored planar map. The order of appearance of the faces is $(1, 2, 3, \hat{1}, \hat{2}, \hat{3})$ clockwise around white vertices and counterclockwise around black vertices (as shown the upper right corner) and, in the presence of *rigid* fully packed loops, we may chose the numbering so that the loops always separate faces labelled 1 from faces labelled $\hat{3}$ and faces labelled $\hat{1}$ from faces labelled 3.
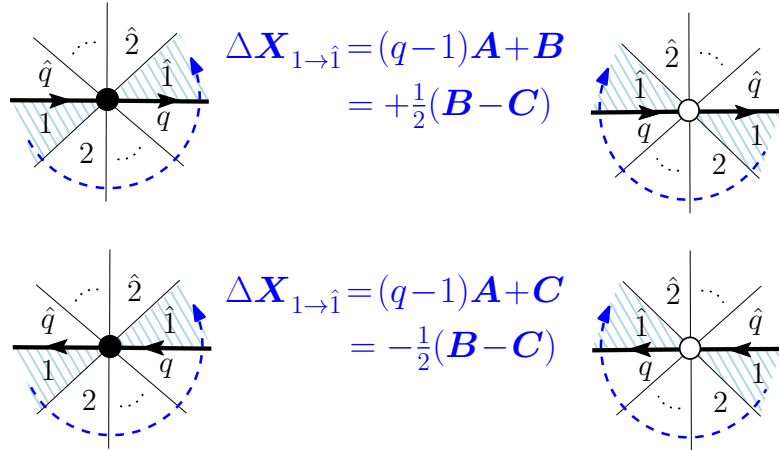
Figure 12: The change of height $\Delta X_{1 \to \hat{1}}$ at a given vertex when going from the face with label 1 to that, opposite, with label $\hat{1}$ is given by $\Delta X_{1 \to \hat{1}} = (q-1)\boldsymbol{A} + \boldsymbol{B}$ or $\Delta X_{1 \to \hat{1}} = (q-1)\boldsymbol{A} + \boldsymbol{C}$ depending on the orientation of the loop. From the relation (19), $\Delta X_{1 \to \hat{1}}$ is therefore equal to $\pm \frac{1}{2}(\boldsymbol{B} - \boldsymbol{C}) = \pm \frac{1}{2}\boldsymbol{b_2}$, with no component along the $\boldsymbol{A}$ direction.

16

Focusing now on the subset $\mathcal{F}_1 \cup \mathcal{F}_{\hat{1}}$, we observe that, as shown in Figure 12, the change of height $\Delta X_{1 \to \hat{1}}$ when going from of the face with label 1 to that with label $\hat{1}$ at a given vertex is always given by

$$\Delta X_{1 \to \hat{1}} = \pm \frac{1}{2} (\boldsymbol{B} - \boldsymbol{C}) = \pm \frac{1}{2} \boldsymbol{b_2} , \qquad (23)$$

with a sign depending on the orientation of the loop. Note finally that, *at any given vertex*, the change of height $\Delta X_{\ell \to \hat{\ell}}$ when going from the incident face with label ℓ to that with label $\hat{\ell}$ is in practice *independent of ℓ*: all in all, the coarse grained height $\boldsymbol{\Psi}$ (whatever its precise definition) has only variations in the $\boldsymbol{b_2}$ direction. $\qquad \square$

5.3. Exact enumeration

The fact that $\gamma = \gamma(-2) = -1$ for rigid Hamiltonian cycles on $2q$-regular bicolored planar maps may be checked by an exact enumeration of the allowed configurations. By embedding the map on the Riemann sphere, i.e., opening the cycle into a straight line of alternating black and white vertices, we immediately see that the rigidity constraints (imposing that the number of unvisited edges incident to any vertex is $(q-1)$ *on each side* of the straight line) allows us to write by symmetry

$$z_N = c_N^2 , \qquad (24)$$

where c_N enumerates configurations of non-crossing bicolored arches connecting the black and white vertices on one side of the straight line only, each vertex being incident to exactly $(q-1)$ arches, see Figure 13-top for an illustration.

As for c_N, it is easily evaluated from the following argument: start by splitting each vertex into $(q-1)$ copies of the same color, with one arch incident to each copy, the choice of the arch to be connected being entirely dictated by the non-crossing constraint of the arches. We now have a sequence made of N groups of $(q-1)$ successive black vertices alternating with N groups of $(q-1)$ successive white vertices. In a given monocolor group of size $(q-1)$, we may label the vertices from 1 to $(q-1)$ from left to right: the non-crossing constraint imposes that a black vertex with label j is necessarily connected to a white vertex with label $(q-j)$ for any $j \in \{1, \ldots, q-1\}$, see Figure 13-middle.

Looking now at the $(q-1)$ first black vertices on the left, denoted by $u_1, \ldots, u_{q-1}$ (so that u_j has the abovementioned label j) and calling v_{q-j} the white vertex to which u_j is connected (so that v_{q-j} has the abovementioned label $(q-j)$), these latter vertices split the remaining $2(q-1)(N-1)$ vertices into subsequences respectively between u_{q-1} and v_1, between v_1 and v_2, $\ldots$, between v_{q-2} and v_{q-1}, and finally to the right of v_{q-1}. This yields a total of q subsequences of non negative integer lengths $2(q-1)m_1, \ldots, 2(q-1)m_q$ respectively with $m_j \geq 0$ for $j = 1, \ldots, q$. Due to the presence of the $(q-1)$ first arches, each of these q subsequences is separated from the others: in particular, the pairing by arches of the vertices takes place independently within each subsequence. Moreover, *at the price of a cyclic permutation* of its vertices, the j-th subsequence is made of m_j groups of $(q-1)$ successive black vertices alternating with m_j groups of $(q-1)$ successive white vertices, see Figure 13-bottom. The number of possible arch configurations for the j-th
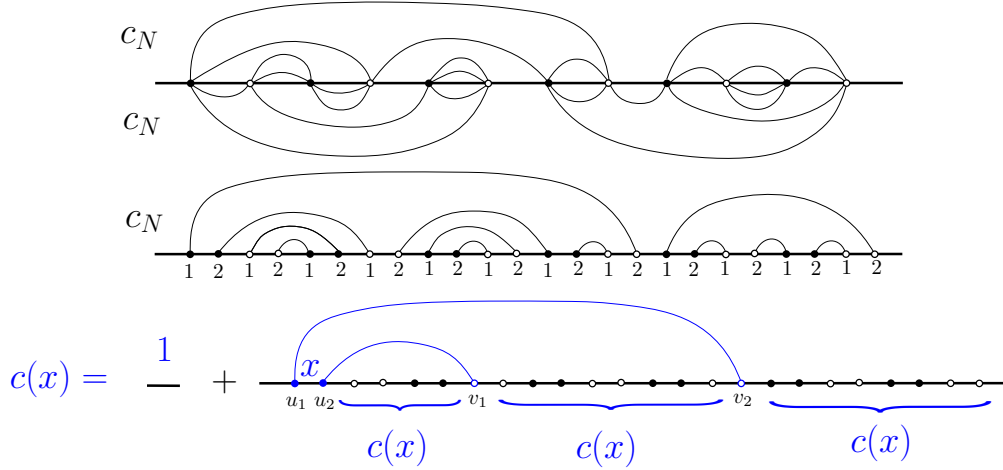
Figure 13: Top: an example of rigid Hamiltonian cycle on a $2q$-valent bicolored planar map (here with $q = 3$), after opening it into a straight line of alternating black and white vertices. The upper and lower parts are independent arch systems, both enumerated by c_N. Middle: alternative representation of the upper arch system after splitting each vertex into $(q-1)$ successive copies of the same color. A black (resp. white) vertex labelled j is connected to a white (resp. black) one labelled $q - j$ (here with $q = 3$ and $j = 1, 2$). Bottom: schematic picture of the decomposition of an arch configuration enumerated by $c(x)$ (with a weight x per group of q arches) into q sequences of arch configurations, each of them also enumerated by $c(x)$. Note that the order of colors within different subsequences is always the same, up to a cyclic permutation.

subsequence is therefore given by c_{m_j} (independently of the required cyclic permutation). We arrive at the recursion relation

$$c_N = \sum_{\substack{m_1,\dots,m_q \geq 0 \\ m_1 + \cdots + m_q = (N-1)}} \prod_{j=1}^{q} c_{m_j} , \quad N \geq 1 \tag{25}$$

with the convention $c_0 = 1$. Introducing the generating function $c(x) := \sum_{N \geq 0} c_N x^N$, we deduce that

$$c(x) = 1 + x \, (c(x))^q , \tag{26}$$

where we recognize the equation determining the generating function $c(x)$ of the q-th generalized Fuss-Catalan numbers [22]

$$c_N = \frac{1}{(q-1)N + 1} \binom{qN}{N} , \quad N \geq 0 . \tag{27}$$

In particular, when $q = 2$, we recover the celebrated Catalan numbers. As a consequence of (27), we get

$$z_N = \left(\frac{1}{(q-1)N + 1} \binom{qN}{N} \right)^2 \underset{N \to \infty}{\sim} \frac{q}{2\pi(q-1)^3} \frac{\left(\frac{q^q}{(q-1)^{q-1}} \right)^{2N}}{N^3} . \tag{28}$$

18

As expected, z_N has the asymptotic behavior (1) with

$$\gamma = \gamma(-2) = -1 \ , \quad \mu = \frac{q^q}{(q-1)^{q-1}} \quad \text{and} \quad \varkappa = \frac{q}{2\pi(q-1)^3} \ . \tag{29}$$

6. Long-distance contacts within Hamiltonian cycles

6.1. Scaling limits of the $\mathrm{O}(n)$ and $\mathrm{FPL}(n)$ models on regular lattices

It is widely believed that the *scaling limit* of the critical $\mathrm{O}(n)$ model on two dimensional regular (e.g., hexagonal or square) lattices is described by the celebrated *Schramm-Loewner evolution* SLE_κ [7, 23], and its collection of critical loops by the so-called *conformal loop ensemble* CLE_κ [24]. This conformally invariant random process depends on a single parameter $\kappa \geq 0$, which in the $\mathrm{O}(n)$ model case is $\kappa = 4/g$ [24, 25, 26, 27] so that :

$$n = -2\cos(4\pi/\kappa), \quad \kappa \in [8/3, 4] \quad \text{for the } \textit{dilute} \text{ critical point,}$$
$$\kappa \in (4, 8] \quad \text{for the } \textit{dense} \text{ critical phase.} \tag{30}$$

For $n \in (0, 2]$, one has $\kappa \in (8/3, 8)$, i.e., the range for which CLE_κ is defined, whereas the SLE_κ process is actually defined for $\kappa \in [0, \infty)$. Note that for $n \to 0$, in the dilute case, the limit of CLE_κ as $\kappa \searrow 8/3$ is $\mathrm{SLE}_{8/3}$ and, in the dense case, the limit of CLE_κ as $\kappa \nearrow 8$ is space-filling SLE_8. The full critical $\mathrm{O}(n)$ model range $n \in [-2, 2]$ corresponds to $\kappa \in [2, \infty)$ SLE_κ paths, which are always non self-crossing, are *simple*, i.e., non-intersecting when $\kappa \in [0, 4]$, and *non-simple* when $\kappa \in (4, \infty)$ [23].

This scaling limit has been rigorously established in several cases: the uniform spanning tree for which $n = 0, g = 1/2, \kappa = 8$ [28]; the loop-erased random walk for which (formally) $n = -2, g = 2, \kappa = 2$ [28, 29]; the contour lines of the discrete Gaussian free field, for which $n = 2, g = 1, \kappa = 4$ [30]; critical site percolation on the triangular lattice [31, 32], for which $n = 1, g = 2/3, \kappa = 6$; the critical Ising model and its associated Fortuin-Kasteleyn random cluster model on the square lattice [33, 34] for which, respectively, $n = 1, g = 4/3, \kappa = 3$ and $n = \sqrt{2}, g = 3/4, \kappa = 16/3$.

The associated SLE_κ central charge is then

$$c = c_{\mathrm{sle}}(\kappa) := \frac{1}{4}(6 - \kappa)\left(6 - \frac{16}{\kappa}\right) \in (-\infty, 1] \quad \text{for} \quad \kappa > 0 \ . \tag{31}$$

Notice the invariance of the central charge (31) under the SLE_κ *duality* [35, 25, 26, 36, 37],

$$\kappa \leftrightarrow 16/\kappa =: \widetilde{\kappa} \ . \tag{32}$$

The geometrical interpretation of this duality is as follows. In the scaling limit, loops in the dense $\mathrm{O}(n)$ model are *non-simple* paths of Hausdorff dimension [38, 39] $D = 1 + (2g)^{-1} = 1 + \kappa/8 > 3/2$ for $g \in [1/2, 1)$, $\kappa \in (4, 8]$; their *external perimeters* are *simple* critical paths of Hausdorff dimension [35] $\widetilde{D} = 1 + g/2 = 1 + \widetilde{\kappa}/8 < 3/2$. These Hausdorff dimensions thus satisfy the universal duality relation

$$(D - 1)(\widetilde{D} - 1) = \frac{1}{4} \ , \tag{33}$$

which has been directly established for critical percolation [40]. Non-simple SLE_κ paths for $\kappa \in (4, 8]$ have indeed been proven to have for outer boundaries dual simple $SLE_{\widetilde{\kappa}}$ paths, with $\widetilde{\kappa} = 16/\kappa \in [2, 4)$ [36, 37].

The so-called *watermelon* exponents (conformal weights) corresponding to the merging of a number ℓ of conformally invariant SLE_κ paths [26], in particular of ℓ critical lines in the (dense or dilute) $O(n)$ model with n as in (30) are given by [38, 39, 41, 42, 43, 44, 45, 46, 47]

$$h_\ell^{(\kappa)} = \frac{1}{16\kappa} \left[4\ell^2 - (4 - \kappa)^2 \right], \quad \ell \in \mathbb{Z}^+. \tag{34}$$

As anticipated above, the Hausdorff dimension of SLE_κ is [48]

$$D = \inf\{2(1 - h_2^{(\kappa)}), 2\} = \inf\{1 + \kappa/8, 2\} . \tag{35}$$

The fully-packed $FPL(n)$ model on the hexagonal lattice [11, 12, 13] or on the square lattice [15, 16] is related to the corresponding dense $O(n)$ model via a shift of its central charge by one unit as in (6) and (11). The watermelon exponents for an *even* number of paths are the same in $FPL(n)$ and dense $O(n)$ models, and in particular the 2-leg exponent which gives the Hausdorff dimension of the paths, whereas those for a *odd* number of paths differ both on the hexagonal ($\bigcirc$) [11, 12, 13], and on the square ($\square$) [15, 16] lattices,

$$
\begin{aligned}
h_{2k}^{\mathrm{fpl}(n)} &= h_{2k}^{(\kappa)}, \\
h_{2k-1}^{\mathrm{fpl}(n)} &= h_{2k-1}^{(\kappa)} + \frac{3}{4\kappa} \quad (\bigcirc), \\
h_{2k-1}^{\mathrm{fpl}(n)} &= h_{2k-1}^{(\kappa)} + \frac{1}{6 + \kappa} \quad (\square), \quad k \in \mathbb{Z}^+.
\end{aligned}
\tag{36}
$$

Even in the presence of the mismatch of central charges (6) and (11), one is thus led to conjecture [1, 8, 9] that the scaling limit of the fully-packed $FPL(n)$ loop model itself on the honeycomb or square lattices is described by a conformal loop ensemble CLE_κ, with κ corresponding to the dense $O(n)$ model phase [10, 11, 12, 13, 15, 16],

$$\kappa = \frac{4\pi}{\arccos(-n/2)} \in (4, 8] \quad \text{for} \quad n \in [0, 2) . \tag{37}$$

6.2. Scaling limit for Hamiltonian cycles

Let us now consider the $FPL(n = 0)$ case of a single Hamiltonian cycle $\mathcal{C}$ with $2N$ vertices, drawn on the regular bicolored hexagonal (or square) lattice, with the sphere topology. Marking two points at distance N along $\mathcal{C}$ splits this cycle into two equal parts $\mathcal{C}_i, i = 1, 2$ such that $\mathcal{C} = \mathcal{C}_1 \cup \mathcal{C}_2$. They are separated by a single closed path $\widetilde{\mathcal{C}}$ drawn on the dual triangular lattice, that crosses the whole set of *contacts links*, i.e., edges incident to a vertex in $\mathcal{C}_1$ and to one in $\mathcal{C}_2$. We write $\widetilde{\mathcal{C}} = \mathcal{C}_1 \cap \mathcal{C}_2$ by a slight abuse of notation. In the spherical topology, this dual path can be viewed as the common external perimeter shared by each of the two halves $\mathcal{C}_i, i = 1, 2$ of $\mathcal{C}$ (see Figure 14).
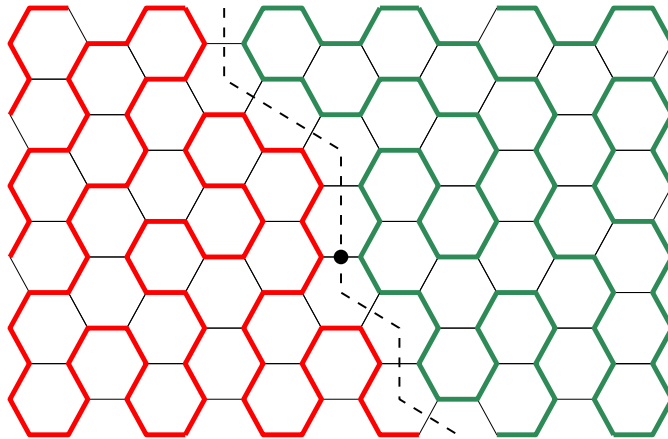
Figure 14: On the hexagonal lattice with the spherical topology, the two (red and green) *halves* $\mathcal{C}_1$ and $\mathcal{C}_2$ of a *Hamiltonian cycle* $\mathcal{C} = \mathcal{C}_1 \cup \mathcal{C}_2$ are separated by a (dotted) dual loop $\widetilde{\mathcal{C}} = \mathcal{C}_1 \cap \mathcal{C}_2$ on the dual lattice that crosses the whole set of their *contact links*. This separatrix can be seen as the *external perimeter* of each half of $\mathcal{C}$. A point along that dual loop can be viewed as the origin of either $\ell = 4$ compact $O(n = 0)$ half-lines, or of $\ell = 2$ dual half-lines. In the scaling limit, the fully-packed loop $\mathcal{C}$ converges to space-filling $\mathrm{SLE}_{\kappa=8}$ with Hausdorff dimension $D = 2$, and its fractal contact set $\widetilde{\mathcal{C}}$ to whole-plane $\mathrm{SLE}_{\widetilde{\kappa}=2}$, with Hausdorff dimension $\widetilde{D} = 5/4$.

In the scaling limit, one has $g = 1/2, \kappa = 8$, so the cycle $\mathcal{C}$ should converge to a *conformally invariant* SLE_8 path drawn on the Riemann sphere, which is a *Peano curve*, i.e., a space-filling curve with Hausdorff dimension $D = 2$. By duality (32) (33), the path $\widetilde{\mathcal{C}}$ should then converge to a whole-plane SLE_2 curve with Hausdorff dimension $\widetilde{D} = 5/4$.

This can be directly checked by observing that a contact point on $\widetilde{\mathcal{C}}$ can be viewed as the origin of $\ell = 4$ fully-packed $n = 0$ lines, i.e., in the scaling limit, that of $\ell = 4$ space-filling SLE_8 paths, as well as the origin of $\ell = 2$ SLE_2 dual paths, with identical conformal weights (34)

$$h_{1 \cap 2} := h_{\ell=4}^{\mathrm{fpl}(0)} = h_{\ell=4}^{(\kappa=8)} = h_{\ell=2}^{(\widetilde{\kappa}=2)} = \frac{3}{8} \ . \tag{38}$$

The expected number $|\widetilde{\mathcal{C}}| = |\mathcal{C}_1 \cap \mathcal{C}_2|$ of contact links between the two halves of Hamiltonian cycle $\mathcal{C}$, in a large domain $\mathcal{D}$ of area $A = |\mathcal{D}|$ on the regular bicolored lattice, is then given, in the scaling limit, by

$$\mathbb{E} |\mathcal{C}_1 \cap \mathcal{C}_2| \asymp A^{\widetilde{D}/2} = A^{1-h_{1\cap2}}, \ \ h_{1\cap2} = 3/8, \quad A \to \infty \ , \tag{39}$$

where the asymptotic equivalence $\asymp$ means that the ratio of logarithms tends to 1.

6.3. Coupling to quantum gravity

Random planar maps, as weighted by the partition functions of critical statistical models, are widely believed to have for scaling limits *Liouville quantum gravity* (LQG) coupled to

the conformal field theory describing these critical models [2, 3, 4], or, equivalently, to the corresponding SLE processes [49, 50, 51, 6]. The continuum description of the random planar map area involves a (regularized) Liouville quantum measure $d^2x\ :\ e^{\gamma_L\varphi_L(x)}\ :$ in terms of a Gaussian free field (GFF) φ_L [52], possibly weighted as in the Liouville action [2, 3, 4]. For the coupling to gravity of a CFT with central charge c, the Liouville parameter γ_L is [2, 3, 4, 6, 49, 50, 51]

$$\gamma_L = \gamma_L(c) := \frac{1}{\sqrt{6}}\left(\sqrt{25-c}-\sqrt{1-c}\right) \in (0,2] \quad \text{for} \quad c \in (-\infty, 1] \ . \tag{40}$$

An Euclidean fractal measure associated with a set of Hausdorff dimension $D = 2(1-h)$ is transformed in LQG into a quantum fractal measure, via a local multiplicative factor of the form $: e^{\alpha\varphi_L} :$ with $\alpha := \gamma_L(1-\Delta)$, where the quantum scaling exponent Δ is the analogue of the Euclidean scaling exponent h [3, 4, 51]. It is given by the celebrated KPZ relation [2],

$$\Delta = \Delta(h, c) := \frac{\sqrt{1-c+24\,h}-\sqrt{1-c}}{\sqrt{25-c}-\sqrt{1-c}} \ , \tag{41}$$

in terms of the original scaling exponent h (e.g., conformal weight) of the CFT of central charge c. Eq. (41) can be inverted with the help of the Liouville parameter (40) as the simple quadratic formula,

$$h(\Delta) = \frac{\gamma_L^2}{4}\Delta^2 + \left(1 - \frac{\gamma_L^2}{4}\right)\Delta \ . \tag{42}$$

Its rigorous proof [52, 53, 54, 55] rests on the assumption that the GFF or Liouville field φ_L and (any) random fractal curve (possibly described by a CFT) are *independently* sampled.

The other KPZ result (2) for $\gamma(c)$, the configuration or "string susceptibility exponent"

$$\gamma = 1 - 4/\gamma_L^2, \tag{43}$$

or equivalently (40) for $\gamma_L(c)$, gives the precise coupling between the LQG and CFT or SLE parameters. By substituting the SLE central charge $c = c_{sle}(\kappa)$ (31), one indeed obtains the simple expressions

$$\gamma = 1 - \sup\{4/\kappa, \kappa/4\}, \quad \gamma_L = \inf\{\sqrt{\kappa}, \sqrt{16/\kappa}\} \ . \tag{44}$$

This has been rigorously established in the probabilistic approach by coupling the Gaussian free field in LQG with SLE martingales [49, 51]. In the scaling limit, random cluster models on random planar maps can then be shown to converge (in the so-called peanosphere topology of the mating of trees perspective) to LQG-SLE [6, 56].

This *matching* property (44) of γ, γ_L and κ applies to the scaling limit of the critical, dense or dilute, $O(n)$ model on a random planar map, as well as to the fully-packed FPL(n) model on random (non bicolored) cubic maps [1]. In the case of the fully-packed model on random *bicolored* maps, this also holds in the case of *mixed valencies* (Claim (7)), or in the *rigid* case of $2q$-regular maps (Claim (12)), with

$$c = c_{dense}(n) = c_{sle}(\kappa) \ . \tag{45}$$

However, for random *bicubic* planar maps, as seen in Ref. [1], and for the general *non-rigid* case of *p-regular bicolored* planar maps (Claim (4)), the correspondence (44) no longer holds, and one then has a *mismatch* [8, 9], with (45) replaced in (2), (40) and (41) by

$$c = c_{\mathrm{fpl}}(n) = 1 + c_{\mathrm{sle}}(\kappa) \ , \tag{46}$$

with κ still given by (37). Note that the constraint $c \leq 1$ in the KPZ relations restricts the loop fugacity of the FPL(n) model on a bicubic map to the range $n \in [0, 1]$ with $\kappa \in [6, 8]$, while the complementary range $n \in (1, 2)$ with $\kappa \in (4, 6)$ is likely to correspond to random tree statistics.

A coupling between LQG and SLE with such mismatched parameters has yet to be described rigorously. Following [1], we can simply conjecture here that for $n \in [0, 1]$ the scaling limit of the FPL(n) model on a bicolored p-regular planar map with no rigid condition, will be given by CLE$_\kappa$ [6], with $\kappa \in [6, 8]$ as in (37), on a γ_{L}-LQG sphere with Liouville parameter

$$\gamma_{\mathrm{L}} = \frac{1}{\sqrt{12}} \left(\sqrt{3\left(\kappa + \frac{16}{\kappa}\right) + 22} - \sqrt{3\left(\kappa + \frac{16}{\kappa}\right) - 26} \right) \ , \tag{47}$$

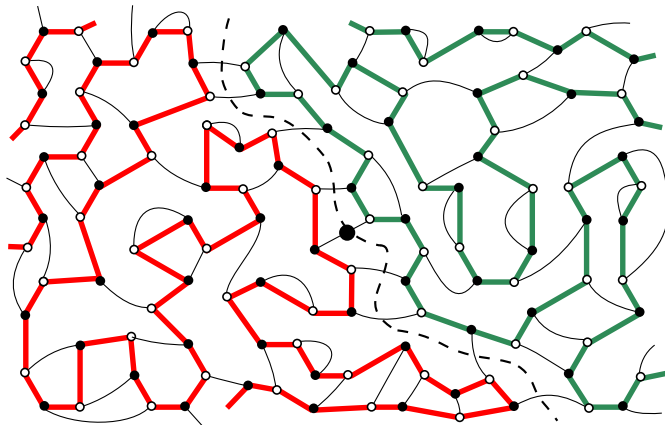in agreement with conjectures proposed in [8, 9].

Figure 15: On a random bicubic planar map with the spherical topology, the two (red and green) halves $\mathcal{C}_1$ and $\mathcal{C}_2$ of a *Hamiltonian cycle* $\mathcal{C} = \mathcal{C}_1 \cup \mathcal{C}_2$ are separated by a (dotted) dual loop $\widetilde{\mathcal{C}} = \mathcal{C}_1 \cap \mathcal{C}_2$ on the dual map that crosses the whole set of their nearest neighbour *contact links*. In the scaling limit, the random map, the fully-packed loop $\mathcal{C}$ and the separatrix $\widetilde{\mathcal{C}}$ converge (in the peanosphere topology [6]) to a γ_{L}-LQG sphere decorated by a space-filling SLE$_8$ and a whole-plane SLE$_2$. In the case of this ($p = 3$)-regular bicolored map, $c = -1$ and $\gamma_{\mathrm{L}} = \frac{1}{\sqrt{3}}\left(\sqrt{13} - 1\right)$.

6.4. Hamiltonian cycles and LQG

The FPL($n = 0$) model on a random planar map converges to space-filling SLE$_{\kappa=8}$ coupled to Liouville quantum gravity, the scaling limit of a Hamiltonian cycle in the

spherical topology being SLE_8 decorating an independent γ_L-LQG sphere (for a proper definition, see [6, 57, 58]), with a Liouville parameter and a central charge depending on the choice of the map's vertex statistics. In the case of generic (i.e., non-bicolored) cubic maps [1], of bicolored maps with vertices of mixed valencies (Corollary (8)), and of $2q$-regular bicolored maps with a local rigidity condition (Corollary(13)), we have from (44) and (45) for $\kappa = 8$,

$$\gamma_L = \sqrt{2}, \quad \gamma = -1, \quad c = -2 \ . \tag{48}$$

In the case of bicubic maps [1] or, more generally, of p-regular bicolored maps (Corollary (5)) we have from (46) and (47) for $\kappa = 8$,

$$\gamma_L = \frac{1}{\sqrt{3}} \left(\sqrt{13} - 1 \right), \quad \gamma = -\frac{1 + \sqrt{13}}{6}, \quad c = -1 \ . \tag{49}$$

Let us consider the set $\widetilde{\mathcal{C}} = \mathcal{C}_1 \cap \mathcal{C}_2$ of contact points between the two halves of the Hamiltonian cycle $\mathcal{C} = \mathcal{C}_1 \cup \mathcal{C}_2$, on a bicolored random planar map of fixed size $2N$ (see Figure 15). In the thermodynamic limit $N \to \infty$, and after rescaling, this set converges (in the peanosphere topology [6]) to the intersection of the two halves of an infinite SLE_8 path, i.e., a whole-plane SLE_2, decorating a quantum sphere of fixed γ_L-LQG area $\mathcal{A}$ [6, 57, 58]. An $SLE_{\kappa=2}$ *quantum length measure* [51, 6] based on the SLE natural parametrization [59] is associated in the scaling limit with the cardinal $|\widetilde{\mathcal{C}}| = |\mathcal{C}_1 \cap \mathcal{C}_2|$. Its expectation scales as

$$\mathbb{E}_{LQG} |\mathcal{C}_1 \cap \mathcal{C}_2| \asymp \mathcal{A}^\nu := \mathcal{A}^{1 - \Delta_{1 \cap 2}} \ , \tag{50}$$

an expression entirely similar to the scaling form (39), but now with a quantum exponent $\Delta_{1 \cap 2} := \Delta(h_{1 \cap 2}, c)$ given by the KPZ relation (41) in terms of $h_{1 \cap 2} = 3/8$ (38). Its value thus crucially depends on the central charge c, i.e., on the choice of vertex statistics on the bicolored map. For case (48), we find

$$\Delta_{1 \cap 2} = \Delta(3/8, c = -2) = 1/2 \ ,$$
$$\nu = 1 - \Delta_{1 \cap 2} = 1/2 \ ; \tag{51}$$

whereas in case (49) we predict

$$\Delta_{1 \cap 2} = \Delta(3/8, c = -1) = \frac{\sqrt{11} - \sqrt{2}}{\sqrt{26} - \sqrt{2}} \ ,$$
$$\nu = 1 - \Delta_{1 \cap 2} = \frac{\sqrt{26} - \sqrt{11}}{\sqrt{26} - \sqrt{2}} = 0.483715 \cdots \ . \tag{52}$$

These two predictions for ν will now be tested numerically using extrapolations from exact enumerations.

7. Numerics for long-distance contacts

Our Hamiltonian cycles have a marked visited edge e. We may thus label all the vertices by their natural order along a cycle $\mathcal{C}$, starting from the black vertex incident to e

(labelled 1) and ending at the white vertex incident to e (labelled $2N$ if the map has size $2N$). This allows us to canonically define the two half-cycles $\mathcal{C}_1$ and $\mathcal{C}_2$ as the parts of $\mathcal{C}$ containing the vertices 1 to N, and $N+1$ to $2N$ respectively. Let us denote by k_N the *average* number of contact links between these two halves of $\mathcal{C}$, see Figure 15. We have

$$k_N = \frac{y_N}{z_N} \tag{53}$$

where y_N denotes the partition function of Hamiltonian cycles (with a marked visited edge) of length $2N$ *weighted by the number of contact links* between their two halves. In the representation of Figure 4, this number of contacts is nothing but the number of (up or down) arches which have been opened along the first half of the straight line and are closed only in its second half. In the transfer matrix formalism, this number is given by the integer parts

$$\lfloor \log_2(\ell_u) \rfloor + \lfloor \log_2(\ell_d) \rfloor \tag{54}$$

where, as in (15), $|\ell_u, \ell_d\rangle$ denotes the "middle" state (i.e., that obtained after the action of N elementary transfer matrices $T_\circ$ or $T_\bullet$). For N even, we may therefore write

$$
\begin{aligned}
y_N &= \sum_{\ell_u, \ell_d} \langle 1,1|(T_\circ T_\bullet)^{N/2}|\ell_u, \ell_d\rangle \big(\lfloor \log_2(\ell_u) \rfloor + \lfloor \log_2(\ell_d) \rfloor \big)\langle \ell_u, \ell_d|(T_\circ T_\bullet)^{N/2}|1,1\rangle \\
&= \sum_{\ell_u, \ell_d} \lfloor \log_2(\ell_u) \rfloor \left(\langle \ell_u, \ell_d|(T_\circ T_\bullet)^{N/2}|1,1\rangle \right)^2 + \sum_{\ell_u, \ell_d} \lfloor \log_2(\ell_d) \rfloor \left(\langle \ell_u, \ell_d|(T_\circ T_\bullet)^{N/2}|1,1\rangle \right)^2 \\
&= 2\sum_{\ell_u, \ell_d} \lfloor \log_2(\ell_u) \rfloor \left(\langle \ell_u, \ell_d|(T_\circ T_\bullet)^{N/2}|1,1\rangle \right)^2 ,
\end{aligned}
\tag{55}
$$

where we used the symmetry of the problem under combined left-right reversal and black-white inversion of colors to go from the first to the second line, as well as its up-down symmetry to go from the second to the third line. For N odd, we have instead

$$y_N = 2\sum_{\ell_u, \ell_d} \lfloor \log_2(\ell_u) \rfloor \left(\langle \ell_u, \ell_d|T_\bullet(T_\circ T_\bullet)^{(N-1)/2}|1,1\rangle \right)^2 . \tag{56}$$

At large N, we expect the asymptotic behavior

$$k_N \underset{N\to\infty}{\sim} \varrho\, N^\nu \tag{57}$$

with ϱ depending on the bicolored map family at hand and with ν as in (51) or (52). We expect however that the corrections to this leading behavior *depend on the parity of N*. This is confirmed by our numerical data: to properly estimate ν from the sequence $(k_N)_{N\geq 1}$, we now have to split this sequence into two subsequences, an "even" one $(k_{2M})_{M\geq 1}$ and an "odd" one $(k_{2M-1})_{M\geq 1}$. This leads us to define the following two independent accelerating series $(\tilde{\nu}_{2M}(s))_{M\geq 1}$ and $(\tilde{\nu}_{2M-1}(s))_{M\geq 1}$:

$$\tilde{\nu}_{2M}(s) = \frac{1}{3!}(\Delta^3 \hat{\nu})_M \quad \text{with} \quad \hat{\nu}_M := M^3\left(M \times \mathrm{Log}\frac{k_{2M+2}+2s}{k_{2M}+2s}\right) \tag{58}$$

and
$$\tilde{\nu}_{2M-1}(s) = \frac{1}{3!}(\Delta^3 \check{\nu})_M \quad \text{with} \quad \check{\nu}_M := M^3 \left(M \times \text{Log} \frac{k_{2M+1} + 2s}{k_{2M-1} + 2s} \right) . \tag{59}$$

Here we introduced for future convenience an arbitrary *shift* parameter s. Both series tends to ν at large M independently of the shift s. The value of s will eventually be fixed numerically for each series so as to optimize the acceleration of the convergence (see below).

It is instructive to start our analysis with the rigid 4-regular case, for which we can write explicit expressions for k_N. We indeed have in this case (see Appendix A)

$$k_{2M} + 2s = \frac{2\binom{2M}{M}^2}{\frac{1}{2M+1}\binom{4M}{2M}} + 2(s-1) ,$$

$$k_{2M-1} + 2s = \frac{2\binom{2M}{M}\binom{2M-2}{M-1}}{\frac{1}{2M}\binom{4M-2}{2M-1}} + 2(s-1) . \tag{60}$$

It is easily checked from these exact expressions that the "even" and "odd" accelerated series $(\tilde{\nu}_{2M}(s))_{M \geq 1}$ and $(\tilde{\nu}_{2M-1}(s))_{M \geq 1}$ do converge to $\nu = 1/2$ as expected, since, at large N, $k_N + 2s \sim 4\sqrt{N/\pi}$ at large N for any fixed s. In order for (58) (resp. (59)) to define a series which is effectively accelerated, i.e., for which the convergence towards ν is fast, it is mandatory that $\hat{\nu}_M$ (resp. $\check{\nu}_M$) have only corrections of the form M^{3-i} for integers $i \geq 1$ so that the first 3 such corrections ($i = 1, 2, 3$) are killed by the 3 iterative finite difference operators Δ . It is easily checked from (60) that, in the present case, this holds only if we choose $s = 1$: for $s \neq 1$, $\hat{\nu}_M$ (resp. $\check{\nu}_M$) also have corrections involving half-integer powers of M, which are not killed by the finite difference operators Δ, leading to a much slower convergence. Otherwise stated, the convergence to $\nu = 1/2$ of $(\tilde{\nu}_{2M}(s))_{M \geq 1}$ (resp. $(\tilde{\nu}_{2M-1}(s))_{M \geq 1}$) is fast and reliable only if we choose $s = 1$.

Suppose now that we do not know the exact expressions (60) and have access only to the first values of $\tilde{\nu}_{2M}(s)$ (resp. $\tilde{\nu}_{2M-1}(s)$) up to some finite value $N_{\max} = 2M_{\max}$ (resp. $N_{\max} = 2M_{\max} - 1$). We may estimate *numerically* the best value s^* of s by demanding that our estimate be stabilized at $N_{\max}$, namely that

$$\tilde{\nu}_{N_{\max}}(s^*) = \tilde{\nu}_{N_{\max}-2}(s^*) . \tag{61}$$

As displayed in Figure 16, using as input the "even" accelerated series for (60) with N up to $N_{\max} = 26$, we obtain numerically the values

$$s^* = 1.000 , \qquad \nu = \tilde{\nu}_{N_{\max}}(s^*) = 0.5000 , \tag{62}$$

in perfect agreement with the values of s^* and ν coming from the above analysis based on the exact asymptotic formulas. This therefore validates a posteriori our numerical recipe (61) for the choice s^* of the shift s.

We have repeated this analysis separately with the "even" data and with the "odd" data for Hamiltonian cycles on various families of bicolored planar maps. For instance, Figure 17 displays our results for 3-regular bicolored maps: we get the estimates

$$s^* = 1.161 , \qquad \nu = \tilde{\nu}_{N_{\max}}(s^*) = 0.4837 , \tag{63}$$
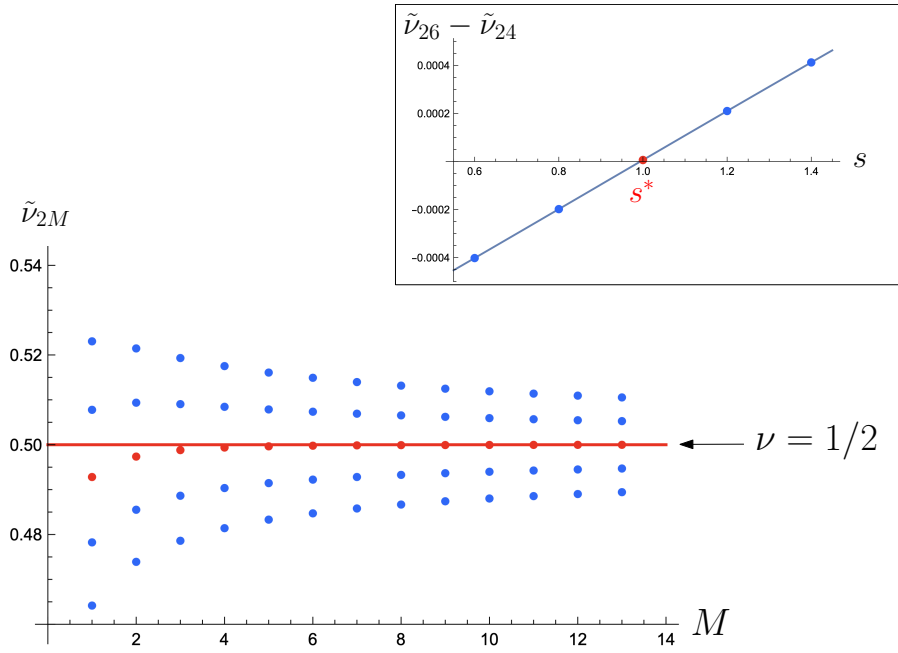
Figure 16: Inset: determination of the shift s^* from the condition $\tilde{\nu}_{N_{\max}}(s^*) = \tilde{\nu}_{N_{\max}-2}(s^*)$ for rigid Hamiltonian cycles on 4-regular bicolored maps (here with $N_{\max} = 26$). We displayed the sequence $(\tilde{\nu}_{2M}(s))_{1 \leq M \leq N_{\max}/2}$ for 5 different values of s. From top to bottom: $s = s^*-0.4$, $s = s^*-0.2$, $s = s^*$ (red), $s = s^*+0.2$ and $s = s^*+0.4$. The value of ν is finally estimated from $\tilde{\nu}_{N_{\max}}(s^*)$ with $s^* = 1.000$, $\nu = \tilde{\nu}_{N_{\max}}(s^*) = 0.5000$

.

Figure 17: Determination of the shift s^* and the exponent ν for Hamiltonian cycles on 3-regular bicolored maps (with $N_{\max} = 26$). See caption of Figure 16 for details.

Figure 18: Determination of the shift s^* and the exponent ν for Hamiltonian cycles on bicolored maps with mixed valencies 2 and 3 (with $N_{\max} = 22$). See caption of Figure 16 for details.
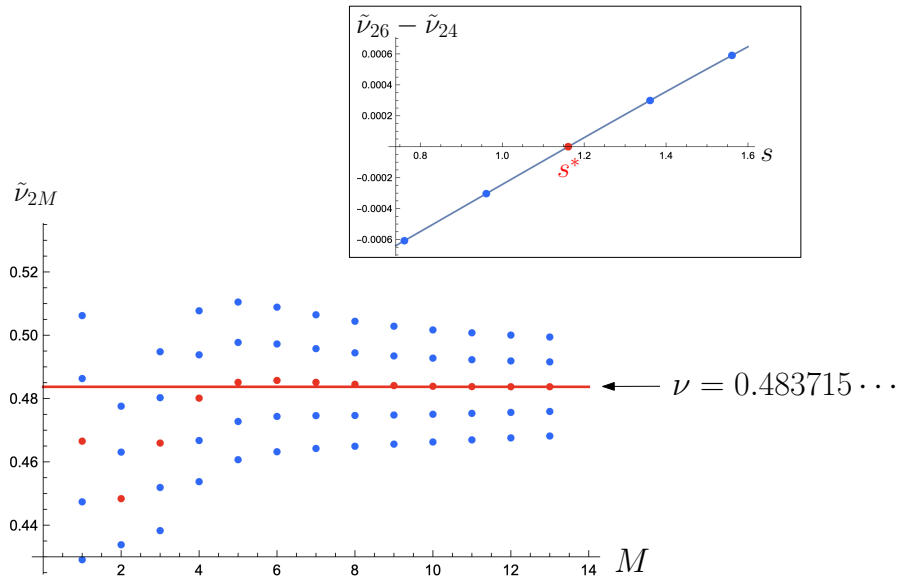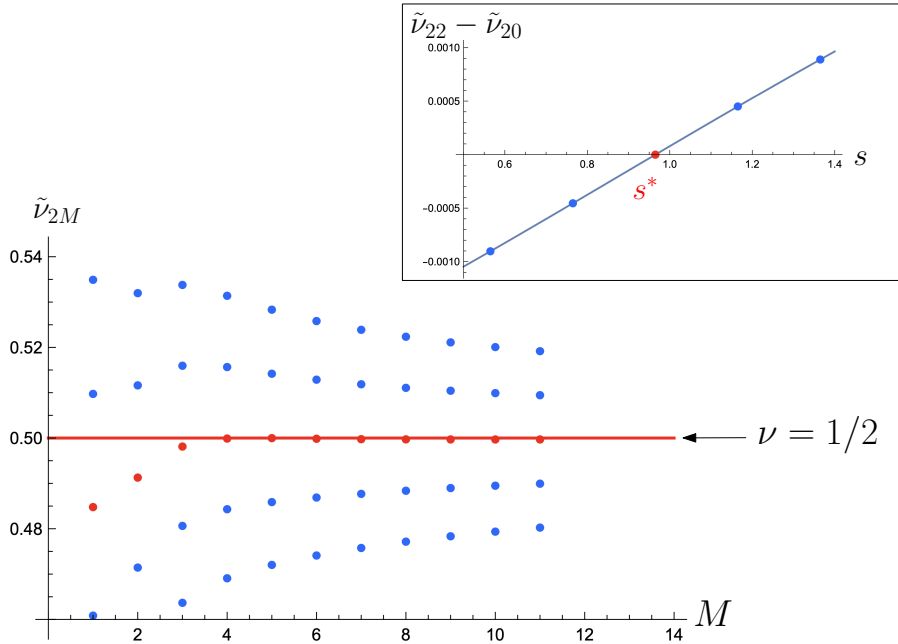
hence a value of ν very close to the predicted value (52). Figure 18 displays similar results for maps with mixed valencies 2 and 3 (and $w_2 = w_3 = 1$), giving now $s^* = 0.965$ and $\nu = 0.4997$ very close to the predicted value $1/2$ of (51). Table 2 gives a summary of our estimates for ν for Hamiltonian cycles on six different bicolored map families and for the two parities of N. All the results are in perfect agreement with the expected values.

8. Conclusion

In this paper, we studied the statistics of Hamiltonian cycles, and more generally of fully packed loops, on various families of bicolored random planar maps and found that the corresponding models fall into two distinct universality classes. The first, most common universality class corresponds to the coupling to gravity of a CFT with central charge $c_{\text{dense}}(n)$ as defined in (11). This universality class is found for fully packed loops on bicolored maps with mixed valencies, for rigid fully packed loops on $2q$-regular bicolored maps, but also for fully packed loops on non-bicolored maps (see Remark 10). It would also be found for non-rigid or rigid dense loops (i.e., $O(n)$ loops in their dense critical phase) on either bicolored or non-bicolored maps. The common feature of all these models is that they can be described by a single height field $\boldsymbol{\Psi} = \psi_2 \boldsymbol{b_2}$. The associated CFT on a regular lattice is that describing the dense phase of the $O(n)$ model, with conformal dimensions which can be computed indifferently on any (hexagonal [39], square [46] or

map family	parity of N	$N_{\max}$	s^*	measured $\nu = \tilde{\nu}_{N_{\max}}(s^*)$	predicted ν
3-regular	even	26	1.161	0.4837	$0.483715\cdots$
	odd	25	1.185	0.4829	
4-regular	even	10	1.008	0.4844	$0.483715\cdots$
	odd	11	1.054	0.4828	
rigid 4-regular	even	$26^\dagger$	1.000	0.5000	0.5
	odd	$25^\dagger$	1.000	0.5000	
rigid 6-regular	even	22	0.817	0.5000	0.5
	odd	21	0.825	0.4999	
mixed valencies 2 and 3	even	22	0.965	0.4997	0.5
	odd	21	0.975	0.4992	
mixed valencies 3 and 4	even	8	0.815	0.4962	0.5
	odd	7	0.855	0.4987	

Table 2: Estimated values of the exponent ν. The value s^* of the shift is determined numerically by the condition $\tilde{\nu}_{N_{\max}}(s^*) = \tilde{\nu}_{N_{\max}-2}(s^*)$. In the cases of mixed valencies, we set $w_2 = w_3 = 1$ (respectively $w_3 = w_4 = 1$). †[For rigid Hamiltonian cycles on 4-regular maps, our explicit expressions (60) allow us to take $N_{\max}$ arbitrarily large. The value 26 (resp. 25) was chosen for a better comparison with the 3-regular case.]

Manhattan [45, 60]) regular lattice. For instance, the watermelon exponent $h_\ell^{(\kappa)}$ is given by (34) for any (even or odd) ℓ, with κ as in (37) and its gravitational counterpart [61, 62, 63, 26] by

$$\Delta\big(h_\ell^{(\kappa)}, c_{\text{sle}}(\kappa)\big) = \frac{\ell}{4} + \frac{1}{8}(4 - \kappa) \ . \tag{64}$$

More interesting is the second universality class, corresponding to the coupling to gravity of a CFT with central charge $c_{\text{fpl}}(n) = 1 + c_{\text{dense}}(n)$ as defined in (6). This universality class is found for fully packed loops on p-regular bicolored maps for any $p \geq 3$, and corresponds to models which may now be described by a two-component height field $\boldsymbol{\Psi} = \psi_1 \boldsymbol{A} + \psi_2 \boldsymbol{b_2}$. In particular, we may cook up observables corresponding to (magnetic) defects (i.e., height dislocations) *with a component along the $\boldsymbol{A}$ direction*: this is the case for instance for watermelon configurations with an *odd number ℓ of lines*.

As already noticed in Section 6, such observables are special in the sense that their conformal weights are different if we compute them on the (naturally bicolored) square and hexagonal regular lattices, see (36). In this sense, universality is not as strong for the second class (with $c = c_{\text{fpl}}(n)$) as it is for the first class and only the spectrum of those observables which *do not involve the $\boldsymbol{A}$ direction* seems to be fully universal: this is in particular the case for the 2- or 4-line observables involved in (38) and associated with the exponent ν that we considered in this paper. As for the special observables (involving the $\boldsymbol{A}$-direction), which seem to retain in the scaling limit a memory of the original lattice, one may wonder about their proper continuous description within the SLE_κ formalism.

When considering the watermelon configurations with an odd number of lines on p-regular bicolored random maps, the fact that there are two possible values for the fully

packed conformal weight $h = h^{\mathrm{fpl}(n)}_{2k-1}$ in (36) casts some doubt on the naive use of the KPZ formula (41) to get the analogue of the dense formula (64). Even when some choice seems "natural" (like for instance that of the hexagonal lattice value in (36) when dealing with 3-regular bicolored maps), it was observed in [1] that the associated gravitational exponent Δ is no-longer directly related to h via the KPZ formula (41) and that some prior "renormalization" of the conformal weight is required.

A subsidiary question about Hamiltonian paths on p-regular bicolored maps is therefore whether such special exponents depend on p, just like they do on regular lattices with $p = 3$ and $p = 4$, hence lead to a weaker notion of universality. We leave this issue for a future work.

Acknowledgements

A. Rigid Hamiltonian cycles on 4-regular bicolored maps: exact enumeration formulas

The case of rigid Hamiltonian cycles on 4-regular bicolored maps (also called meandric systems in [20, 9]) is particularly simple as we may get exact expressions for z_N and y_N, hence for k_N in (53). As already mentioned in Section 5.3, opening the rigid cycle into a straight line of alternating black and white vertices totally decouples the upper and lower parts, implying that

$$z_N = c_N^2 \ , \tag{65}$$

where c_N enumerates non-crossing arch configurations connecting $2N$ vertices along a line *on one side only*. Note that the fact that arches connect vertices of different colors is automatic for non-crossing arch configurations, hence we may forget about the colors in this particular case. As it is well known, c_N is nothing but the celebrated Catalan number

$$c_N = \frac{1}{N+1}\binom{2N}{N} \ , \tag{66}$$

in agreement with (27) for $q = 2$. Let us now discuss the quantity y_N. The decoupling
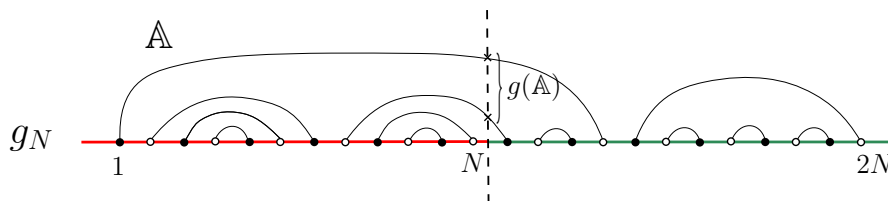

Figure 19: An arch configuration $\mathbb{A}$ contributing to g_N (here with $N = 12$) and the number $g(\mathbb{A})$ of arches passing above the middle point (here $g(\mathbb{A})=2$), whose parity is the same as that of N.

30

of the upper and lower parts (together with the up-down symmetry) implies that

$$y_N = 2g_N c_N \qquad (67)$$

where g_N enumerates arch configurations $\mathbb{A}$ connecting $2N$ vertices along a line *on one side only*, weighted by the number $g(\mathbb{A})$ of arches passing above the middle point of the straight line (i.e., the middle point of the edge connecting the N-th to the $(N+1)$-th vertex), see Figure 19. Let us first assume that N is even and write $N = 2M$. This implies that $g(\mathbb{A})$ is even too. More precisely, for $0 \leq p \leq M$, those arch configurations $\mathbb{A}$ for which $g(\mathbb{A}) = 2p$ are enumerated by[6]

$$\left(\binom{2M}{M+p} - \binom{2M}{M+p+1} \right)^2 = \left(\frac{2p+1}{M+p+1} \binom{2M}{M+p} \right)^2 . \qquad (68)$$

This yields

$$\begin{aligned}
g_N &= \sum_{p=0}^{M} \left(\frac{2p+1}{M+p+1} \binom{2M}{M+p} \right)^2 (2p) \\
&= \sum_{p=0}^{M} \left(\frac{2p+1}{M+p+1} \binom{2M}{M+p} \right)^2 (2p+s) - s\, c_N ,
\end{aligned} \qquad (69)$$

where we used the sum rule $\sum_{p=0}^{M} \left(\frac{2p+1}{M+p+1} \binom{2M}{M+p} \right)^2 = c_N$ for the total number of arch configurations. Noting that

$$\left(\frac{2p+1}{M+p+1} \binom{2M}{M+p} \right)^2 (2p+1) = \Delta_p \left(-\frac{(M+2p^2)}{M} \binom{2M}{M+p}^2 \right) \qquad (70)$$

where Δ_p is the forward finite difference operator in p, we see that the sum in the second line of (69) is telescopic for the choice $s = 1$.

We eventually end up with

$$g_N = \binom{2M}{M}^2 - c_N \quad \text{for } N = 2M , \qquad (71)$$

and

$$k_N = \frac{y_N}{z_N} = \frac{2g_N}{c_N} = \frac{2\binom{2M}{M}^2}{\frac{1}{2M+1}\binom{4M}{2M}} - 2 \quad \text{for } N = 2M . \qquad (72)$$

If we now assume that N is odd, a similar calculation leads to

$$k_N = \frac{2\binom{2M}{M}\binom{2M-2}{M-1}}{\frac{1}{2M}\binom{4M-2}{2M-1}} - 2 \quad \text{for } N = 2M - 1 . \qquad (73)$$

Eqs. (72) and (73) lead to the desired formulas (60).

---

[6]In the Dyck path representation of non-crossing arch systems [64], these configurations correspond to pairs made of (i) a path of length $2M$ from height 0 to height $2p$ (hence with $M + p$ up-steps) and (ii) a complementary path of length $2M$ from height $2p$ to height 0 (hence with $M + p$ down steps), both paths having only non-negative heights.

B. Numerical data

N	z_N	$y_N/2$
1	2	1
2	8	4
3	40	28
4	228	182
5	1424	1376
6	9520	10256
7	67064	82256
8	492292	657258
9	3735112	5483168
10	29114128	45720644
11	232077344	392225248
12	1885195276	3367237302
13	15562235264	29496561288
14	130263211680	258689070208
15	1103650297320	2303183835424
16	9450760284100	20532423715862
17	81696139565864	185194267822952
18	712188311673280	1672505538588120
19	6255662512111248	15246126785026456
20	55324571848957688	139146249302900840
21	492328039660580784	1279654964632731016
22	4406003100524940624	11781309072368013800
23	39635193868649858744	109156077594746888256
24	358245485706959890508	1012371771569816836390
25	3252243000921333423544	9439721149094472748640
26	29644552626822516031040	88100169337671128409824
27	271230872346635464906816	826012547472307809557896
28	2490299924154166673782584	7751024033279177862804200
29	22939294579586403144527440	73022459752163336202562352
30	211949268051816569236796848	688468559155925660846596544
31	1963919128426791258770276024	6513579576440364032532422976
32	18246482008315207478524287044	61667572983605062268400200798
33	169953210523325203868381657400	585630198026539853341680121888
34	1586759491069775179474823509344	5565011094981145493511752402704

Table 3: Values of z_N (sequence A116456 in OEIS [65]) and y_N for Hamiltonian cycles on bicolored 3-regular planar maps.

N	z_N	$y_N/2$
1	3	3
2	34	34
3	583	797
4	12370	18962
5	299310	541218
6	7914962	15658990
7	223112249	492077299
8	6599227954	15610597634
9	202656932134	519177791710
10	6413548643796	17387351622688
11	208040580206216	600403799410348
12	6888733433298402	20842604582620710
13	232117149975205154	739230697828101014
14	7939206408814949506	26327452538168278582
15	275098365065617821621	952653521434740072227
16	9641385973628938712306	34586535913246138331782
17	341313811643888153301006	1271131209796113395573406
18	12191280053256623302185704	46844535638524226902706228
19	438954593201892408379178942	1743184882186466069552567270

Table 4: Values of z_N and y_N for Hamiltonian cycles on bicolored 4-regular planar maps.

N	5-regular	6-regular	7-regular
1	4	5	6
2	104	259	560
3	4640	25094	104024
4	266084	3192155	25715048
5	17669760	474183765	7462790096
6	1292292432	77907665840	2401948332096
7	101201942512	13740308705438	831180015105160
8	8340015146964	2554205527336363	303462839364701128
9	714995787362600	494475099243189329	115462177891927344416
10	63259444105430512	98867302126812855515	
11	5742719613679409832	20294465583102673352590	
12	532599319939460085760		
13	50295898068432583524224		
14	4823733144104904305892304		

Table 5: Values of z_N for Hamiltonian cycles on bicolored 5-regular, 6-regular and 7-regular planar maps.

N	z_N	$y_N/2$
1	3	1
2	17	6
3	125	67
4	1077	676
5	10335	8047
6	107151	93898
7	1176999	1184387
8	13518677	14869772
9	160872323	195389839
10	1970329025	2566924518
11	24715305741	34751956495
12	316322082895	471076136766
13	4118646279649	6523535179149
14	54428554176853	90491263299716
15	728662270487961	1275474547319661
16	9866887839946229	18009066127518820
17	134967673222112567	257454410282564295
18	1862969746410518745	3686602712849035850
19	25924506623086706277	53316166797618448047
20	363415643231059957421	772238458092154850980
21	5128518034166712107763	11276238109326334073237
22	72814980427431398768943	164883291621449041519854
23	1039603583945087464438759	2427283275342458095362671
24	14918925552410770296750503	35777211288494249743148062
25	215108422239328159518817305	530360761101151938386907819
26	3115114976238433506239203399	7870933845679033785904203612
27	45295058700528813260672278919	117382878931669305354337886003
28	661097024940535265310437647345	1752373351490083766149516091464
29	9682937008170057158267261746831	26271697196196181749006295843637
30	142290916972981046011294091297071	394231951670046541461277392969298
31	2097420196208084754056265923088015	5937785334543529526068890061788573

Table 6: Values of z_N and y_N for Hamiltonian cycles on bicolored planar maps with mixed valencies 2 and 3 (with $w_2 = w_3 = 1$).

N	z_N	N	z_N
1	4	10	24584694155437
2	47	11	930530200722914
3	872	12	36039351335158162
4	20579	13	1423250588260168692
5	562346	14	57153474076536198864
6	16959202	15	2328611379453123805998
7	549029380	16	96085895789053111221723
8	18750074923	17	4009433404474389044318028
9	667653126308	18	168976691280496979237329801

Table 7: Values of z_N for Hamiltonian cycles on bicolored planar maps with mixed valencies 2 and 4 (with $w_2 = w_4 = 1$).

N	z_N	$y_N/2$
1	5	4
2	98	80
3	3089	3572
4	124622	163552
5	5844034	9159648
6	303138220	522941716
7	16901630655	32699927584
8	994850903414	2071909682642
9	61080867353216	138275419169022
10	3878907227559258	9315849112395598
11	253224873797465540	649064156160267680
12	16915976848381443504	45541980819371884184
13	1152241256370476649482	3271499179479967664002
14	79806203708523623827632	236287877905404626333174
15	5608021949255349143950993	17365297252695426225180534
16	399909547504487281701351142	1281725711268335772862571494

Table 8: Values of z_N and y_N for Hamiltonian cycles on bicolored planar maps with mixed valencies 3 and 4 (with $w_3 = w_4 = 1$).

As already seen in Section 5 (Eqs. (24) (27)) and in Appendix A when $q = 2$, using the arch representation such as that of Figure 4 in the case of *rigid* Hamiltonian cycles on $2q$-regular bicolored planar maps for arbitrary $q \geq 2$ leads to a complete decoupling between the upper and lower arch configurations. This implies the following the two identities (extending (65) and (67)):

$$z_N = c_N^2 \quad \text{with } c_N = \frac{1}{(q-1)N + 1} \binom{q\,N}{N} \tag{74}$$

and

$$y_N = 2g_N c_N \ , \tag{75}$$

where g_N enumerates arch configurations *on one side only*, weighted by the number of arches passing above the middle point of the straight line, see Figure 19 when $q = 2$. We have no exact expression for g_N for arbitrary $q \geq 3$ (which would generalize (71)). The following table gives the first values of g_N in the case $q = 3$, from which we can get y_N via (75).

N	g_N	N	g_N
1	2	16	429765359266
2	6	17	2747996363358
3	32	18	17558452105246
4	162	19	112880676289328
5	930	20	725294746632006
6	5260	21	4683479629941570
7	31432	22	30229921171815208
8	186606	23	195925602453080976
9	1142582	24	1269396826660493508
10	6971466	25	8252873289420323592
11	43385904	26	53640502233395278680
12	269429292	27	349671835181599650032
13	1696338360	28	2278921678933838458548
14	10665144516	29	14890267787292439785072
15	67735129000	30	97273104239590589753820

Table 9: Values of g_N (such that $y_N = 2g_N c_N$ with c_N as in (74)) for rigid Hamiltonian cycles on 6-regular bicolored planar maps (i.e., $q = 3$).

References

[1] Philippe Di Francesco, Bertrand Duplantier, Olivier Golinelli, and Emmanuel Guitter. Exponents for Hamiltonian paths on random bicubic maps and KPZ. *Nuclear Physics B*, 987:116084, 2023.

[2] V.G. Knizhnik, A.M. Polyakov, and A.B. Zamolodchikov. Fractal structure of 2d—quantum gravity. *Modern Physics Letters A*, 03(08):819–826, 1988.

[3] F. David. Conformal field theories coupled to 2-d gravity in the conformal gauge. *Modern Physics Letters A*, 03(17):1651–1656, 1988.

[4] Jacques Distler and Hikaru Kawai. Conformal field theory and 2d quantum gravity. *Nuclear Physics B*, 321(2):509–527, 1989.

[5] E. Guitter, C. Kristjansen, and J.L. Nielsen. Hamiltonian cycles on random Eulerian triangulations. *Nuclear Physics B*, 546(3):731–750, 1999.

[6] Bertrand Duplantier, Jason Miller, and Scott Sheffield. Liouville Quantum Gravity as a mating of trees. *Astérisque.*, 427:1–258, 2021.

[7] Oded Schramm. Scaling limits of loop-erased random walks and uniform spanning trees. *Israel J. Math.*, 118:221–288, 2000.

[8] Jacopo Borga, Ewain Gwynne, and Xin Sun. Permutons, meanders, and SLE-decorated Liouville quantum gravity. *arXiv:2207.02319 [math.PR]*, 2022.

[9] Jacopo Borga, Ewain Gwynne, and Minjae Park. On the geometry of uniform meandric systems. *arXiv:2212.00534 [math.PR]*, 2022.

[10] N. Y. Reshetikhin. A new exactly solvable case of an O(n)-model on a hexagonal lattice. *Journal of Physics A: Mathematical and General*, 24(10):2387, May 1991.

[11] H. W. J. Blöte and B. Nienhuis. Fully packed loop model on the honeycomb lattice. *Phys. Rev. Lett.*, 72:1372–1375, Feb 1994.

[12] M. T. Batchelor, J. Suzuki, and C. M. Yung. Exact results for Hamiltonian walks from the solution of the fully packed loop model on the honeycomb lattice. *Phys. Rev. Lett.*, 73:2646–2649, Nov 1994.

[13] Jane Kondev, Jan de Gier, and Bernard Nienhuis. Operator spectrum and exact exponents of the fully packed loop model. *Journal of Physics A: Mathematical and General*, 29(20):6489–6504, Oct 1996.

[14] P. Di Francesco and E. Guitter. Geometrically constrained statistical systems on regular and random lattices: From folding to meanders. *Physics Reports*, 415(1):1–88, 2005.

[15] M. T. Batchelor, H. W. J. Blöte, B. Nienhuis, and C. M. Yung. Critical behaviour of the fully packed loop model on the square lattice. *Journal of Physics A: Mathematical and General*, 29(16):L399, aug 1996.

[16] Jesper Lykke Jacobsen and Jane Kondev. Field theory of compact polymers on the square lattice. *Nuclear Physics B*, 532(3):635–688, 1998.

[17] David Dei Cont and Bernard Nienhuis. The packing of two species of polygons on the square lattice. *Journal of Physics A: Mathematical and General*, 37(9):3085, feb 2004.

[18] J. Jacobsen and P. Zinn-Justin. Algebraic Bethe Ansatz for the FPL^2 model. *Journal of Physics A: Mathematical and General*, 37(29):7213, jul 2004.

[19] G. Borot, J. Bouttier, and E. Guitter. A recursive approach to the O(n) model on random maps via nested loops. *Journal of Physics A: Mathematical and Theoretical*, 45(4):045002, dec 2011.

[20] Valentin Féray and Paul Thévenin. Components in Meandric Systems and the Infinite Noodle. *International Mathematics Research Notices*, 07 2022. rnac156.

[21] Mireille Bousquet-Mélou and Gilles Schaeffer. Enumeration of planar constellations. *Advances in Applied Mathematics*, 24(4):337–368, 2000.

[22] Nikolaus Fuss. Solutio quæstionis, quot modis polygonum n laterum in polygona m laterum, per diagonales resolvi queat. *Nova Acta Academiae Scientiarum Imperialis Petropolitanae*, 9:243–251, 1793. `https://www.math.ucla.edu/~pak/lectures/Cat/Fuss1.pdf`.

[23] Steffen Rohde and Oded Schramm. Basic properties of SLE. *Ann. of Math. (2)*, 161(2):883–924, 2005.

[24] Scott Sheffield. Exploration trees and conformal loop ensembles. *Duke Mathematical Journal*, 147(1):79 – 129, 2009.

[25] Bertrand Duplantier. Higher conformal multifractality. *J. Stat. Phys.*, 110(3-6):691–738, 2003.

[26] B. Duplantier. Conformal fractal geometry & boundary quantum gravity. In M. L. Lapidus and M. van Frankenhuysen, editors, *Fractal geometry and applications: a jubilee of Benoît Mandelbrot, Part 2*, volume 72 of *Proc. Sympos. Pure Math.*, pages 365–482. Amer. Math. Soc., Providence, RI, 2004.

[27] Wouter Kager and Bernard Nienhuis. A guide to stochastic Löwner evolution and its applications. *J. Stat. Phys.*, 115(5-6):1149–1229, 2004.

[28] Gregory F. Lawler, Oded Schramm, and Wendelin Werner. Conformal invariance of planar loop-erased random walks and uniform spanning trees. *Annals Probab.*, 32:939–995, 2004.

[29] Gregory F. Lawler and Fredrik Viklund. Convergence of loop-erased random walk in the natural parameterization. *Duke Mathematical Journal*, 170(10):2289 – 2370, 2021.

[30] Oded Schramm and Scott Sheffield. Contour lines of the two-dimensional discrete Gaussian free field. *Acta Mathematica*, 202(1):21 – 137, 2009.

[31] Stanislav Smirnov. Critical percolation in the plane: conformal invariance, Cardy's formula, scaling limits. *Comptes Rendus de l'Académie des Sciences - Series I - Mathematics*, 333(3):239–244, 2001.

[32] Federico Camia and Charles M. Newman. Two-dimensional critical percolation: The full scaling limit. *Commun. Math. Phys.*, 268(1):1–38, Nov 2006.

[33] Stanislav Smirnov. Conformal invariance in random cluster models. I: Holomorphic fermions in the Ising model. *Ann. Math.*, 172(2):1435–1467, 2010.

[34] Dmitry Chelkak and Stanislav Smirnov. Universality in the 2d Ising model and conformal invariance of fermionic observables. *Invent. Math.*, 189(3):515 – 580, 2012.

[35] Bertrand Duplantier. Conformally invariant fractals and potential theory. *Phys. Rev. Lett.*, 84(7):1363–1367, 2000.

[36] Dapeng Zhan. Duality of chordal SLE. *Invent. Math.*, 174(2):309–353, 2008.

[37] Julien Dubédat. Duality of Schramm-Loewner evolutions. *Ann. Sci. Éc. Norm. Supér. (4)*, 42(5):697–724, 2009.

[38] Bernard Nienhuis. Exact critical point and critical exponents of O(n) models in two dimensions. *Phys. Rev. Lett.*, 49(15):1062–1065, 1982.

[39] Bernard Nienhuis. Critical behavior of two-dimensional spin models and charge asymmetry in the Coulomb gas. *J. Stat. Phys.*, 34:731–762, 1984.

[40] Michael Aizenman, Bertrand Duplantier, and Amnon Aharony. Path-crossing exponents and the external perimeter in 2d percolation. *Phys. Rev. Lett.*, 83:1359–1362, 1999.

[41] Bernard Nienhuis. Coulomb gas formulation of two-dimensional phase transitions. In C. Domb, M. Green, and J. Lebowitz, editors, *Phase transitions and critical phenomena, Vol. 11*, pages 1–53. Academic Press, London, 1987.

[42] H. Saleur. New exact exponents for two-dimensional self-avoiding walks. *Journal of Physics A: Mathematical and General*, 19(13):L807–L810, 1986.

[43] B. Duplantier. Exact critical exponents for two-dimensional dense polymers. *Journal of Physics A: Mathematical and General*, 19(16):L1009–L1014, 1986.

[44] B. Duplantier and H. Saleur. Exact critical properties of two-dimensional dense self-avoiding walks. *Nuclear Physics B*, 290(3):291–326, 1987.

[45] Bertrand Duplantier. Critical exponents of Manhattan Hamiltonian walks in two dimensions, from Potts and O(n) models. *J. Stat. Phys.*, 49(3-4):411–431, 1987.

[46] H. Saleur and B. Duplantier. Exact determination of the percolation hull exponent in two dimensions. *Phys. Rev. Lett.*, 58:2325–2328, 1987.

[47] Murray T. Batchelor and Henk W. J. Blöte. Conformal anomaly and scaling dimensions of the O(n) model from an exact solution on the honeycomb lattice. *Phys. Rev. Lett.*, 61:138–140, 1988.

[48] Vincent Beffara. The dimension of the SLE curves. *Ann. Probab*, 36(4):1421 – 1452, 2008.

[49] Scott Sheffield. Conformal weldings of random surfaces: SLE and the quantum gravity zipper. *Ann. Probab.*, 44(5):3474 – 3545, 2016.

[50] Scott Sheffield. Quantum gravity and inventory accumulation. *Ann. Probab.*, 44(6):3804 – 3848, 2016.

[51] B. Duplantier and S. Sheffield. Schramm-Loewner Evolution and Liouville Quantum Gravity. *Phys. Rev. Lett.*, 107:131305, 2011.

[52] B. Duplantier and S. Sheffield. Liouville Quantum Gravity and KPZ. *Invent. Math.*, 185:333–393, 2011.

[53] B. Duplantier and S. Sheffield. Duality and KPZ in Liouville Quantum Gravity. *Phys. Rev. Lett.*, 102:150603, 2009.

[54] R. Rhodes and V. Vargas. KPZ formula for log-infinitely divisible multifractal random measures. *ESAIM: Probability and Statistics*, 15:358–371, 2011.

[55] Bertrand Duplantier, Rémi Rhodes, Scott Sheffield, and Vincent Vargas. Renormalization of critical Gaussian multiplicative chaos and KPZ relation. *Commun. Math. Phys.*, 330(1):283 – 330, 2014.

[56] Ewain Gwynne, Nina Holden, and Xin Sun. Mating of trees for random planar maps and Liouville quantum gravity: a survey. *arXiv:1910.04713 [math.PR]*, 2019. Panorama et Synthèses, to appear).

[57] François David, Antti Kupiainen, Rémi Rhodes, and Vincent Vargas. Liouville quantum gravity on the Riemann sphere. *Commun. Math. Phys.*, 342(3):869–907, 2016.

[58] Juhan Aru, Yichao Huang, and Xin Sun. Two Perspectives of the 2D Unit Area Quantum Sphere and Their Equivalence. *Commun. Math. Phys.*, 356(1):261–283, 2017.

[59] Gregory F. Lawler and Scott Sheffield. A natural parametrization for the Schramm-Loewner evolution. *Ann. Probab.*, 39(5):1896–1937, 2011.

[60] Bertrand Duplantier and François David. Exact partition functions and correlation functions of multiple hamiltonian walks on the Manhattan lattice. *J. Stat. Phys.*, 51(3):327–434, 1988.

[61] Bertrand Duplantier and Ivan Kostov. Conformal spectra of polymers on a random surface. *Phys. Rev. Lett.*, 61:1433–1437, 1988.

[62] Bertrand Duplantier and Ivan K. Kostov. Geometrical Critical Phenomena on a Random Surface of Arbitrary Genus. *Nuclear Physics B*, 340:491–541, 1990.

[63] I. K. Kostov. O(n) vector model on a planar random lattice: Spectrum of anomalous dimensions. *Modern Physics Letters A*, 04(03):217–226, 1989.

[64] Richard P. Stanley. *Catalan Numbers*. Cambridge University Press, 2015.

[65] The OEIS Foundation Inc. The on-line encyclopedia of integer sequences, published electronically at http://oeis.org, 2023.